Hydrol. Earth Syst. Sci. Discuss., 10, 5397–5456, 2013
www.hydrol-earth-syst-sci-discuss.net/10/5397/2013/
doi:10.5194/hessd-10-5397-2013

Hydrology and Earth System Sciences
Open Access
Discussions

Changes of evapotranspiration and water yield in China's terrestrial ecosystems during the period from 2000 to 2010

Y. Liu[1,2], Y. Zhou[1,3], W. Ju[1,2], J. Chen[1,2], S. Wang[4], H. He[4], H. Wang[4], D. Guan[5], F. Zhao[4], Y. Li[6], and Y. Hao[7]

[1]Jiangsu Provincial Key Laboratory of Geographic Information Science and Technology, Nanjing University, Nanjing, 210023, China
[2]International Institute for Earth System Sciences, Nanjing University, Nanjing, 210023, China
[3]School of Geographic and Oceanographic Sciences, Nanjing University, Nanjing, 210023, China
[4]Key Laboratory of Ecosystem Network Observation and Modeling, Institute of Geographic Sciences and Natural Resources Research, Chinese Academy of Sciences, Beijing, 100101, China
[5]Institute of Applied Ecology, Chinese Academy of Sciences, Shenyang, 110016, China
[6]Northwest Institute of Plateau Biology, Chinese Academy of Sciences, Xining, 810008, China
[7]Graduate University of Chinese Academy of Sciences, Beijing, 100049, China

Received: 5 March 2013 – Accepted: 15 April 2013 – Published: 29 April 2013

Correspondence to: Y. Zhou (zhouyl@nju.edu.cn)

Published by Copernicus Publications on behalf of the European Geosciences Union.

HESSD
10, 5397–5456, 2013

Abstract

Terrestrial carbon and water cycles are interactively linked at various spatial and temporal scales. Evapotranspiration (ET) plays a key role in the terrestrial water cycle and altering carbon sequestration of terrestrial ecosystems. The study of ET and its response to climate and vegetation changes is critical in China since water availability is a limiting factor for the functioning of terrestrial ecosystems in vast arid and semi-arid regions. In this study, the process-based Boreal Ecosystem Productivity Simulator (BEPS) model was employed in conjunction with a newly developed leaf area index (LAI) dataset and other spatial data to simulate daily ET and water yield at a spatial resolution of 500 m over China for the period from 2000 to 2010. The spatial and temporal variations of ET and water yield and influences of temperature, precipitation, land cover types, and LAI on ET were analyzed.

The validations with ET measured at 5 typical ChinaFLUX sites and inferred using statistical hydrological data in 10 basins showed that the BEPS model was able to simulate daily and annual ET well at site and basin scales. Simulated annual ET exhibited a distinguishable southeast to northwest decreasing gradient, corresponding to climate conditions and vegetation types. It increased with the increase of LAI in 74 % of China's landmass and was positively correlated with temperature in most areas of southwest, south, east, and central China and with precipitation in the arid and semi-arid areas of northwest and north China. In the Tibet Plateau and humid southeast China, the increase in precipitation might cause ET to decrease. The national mean annual ET varied from 345.5 mm yr^{-1} in 2001 to 387.8 mm yr^{-1} in 2005, with an average of 369.8 mm yr^{-1} during the study period. The overall increase rate of 1.7 mm yr^{-2} (r = 0.43 p = 0.19) was mainly driven by the increase of total ET in forests. During the period from 2006 to 2009, precipitation and LAI decreased widely and consequently caused a detectable decrease of national total ET. The temporal patterns of ET varied spatially during the 11 yr study period, increasing in 62.2 % of China's landmass, especially in the cropland areas of southern Haihe river basin, most of the Huaihe river

HESSD
10, 5397–5456, 2013

basin, and southeastern Yangtze river basin. Decreases of annual ET mainly occurred in parts of northeast, north, northwest, south China, especially in eastern Qinghai-Tibet plateau, the south part of Yunnan province, and Hainan province. Vast regions in China, especially the regions south of Yangtze river, experienced significant decreases in water yield caused by the reduction of precipitation and increase of ET while some areas sporadically distributed in northeast, east, northwest, central, and south China experienced increases in water yield. This study shows that recent climatic variability and human activity induced vegetations changes have intensified the terrestrial water cycles in China's terrestrial ecosystems, which is worthy of further thorough investigation.

1 Introduction

The terrestrial hydrological cycle is essential for the functioning and sustainability of earth systems (Hutjes et al., 1998). Understanding its spatial and temporal variations and underlying driving factors are fundamental for predicting the response and feedback of terrestrial ecosystems to global changes. As one of the most important components within the terrestrial hydrological cycle, evapotranspiration (ET) links the hydrological, energy, and carbon cycles (Fisher et al., 2008; Jung et al., 2010). Globally, terrestrial ET processes consume more than 50 % of the solar radiation absorbed by the land surface (Trenberth et al., 2009), and affect precipitation by returning approximately 60 % of the annual land precipitation back to the atmosphere (Koster et al., 2004; Oki and Kanae, 2006).

Previous studies have indicated that climate change might cause more frequent floods and droughts (Huntington, 2006). Further warming will further promote this trend (Meehl and Tebaldi, 2004). Accurately estimating the spatial and temporal variations of ET is critical for better understanding the interactions between the atmosphere and land surface, and improving water resource management and drought assessment under climate change (Jung et al., 2010; Yuan et al., 2010; Fisher et al., 2011; Yan et al.,

HESSD
10, 5397–5456, 2013

2012; Zeng et al., 2012). However, ET is the most difficult component of the terrestrial water cycle to estimate accurately because of the heterogeneity of the landscape and numerous controlling factors, including climate, plant biophysics, soil properties, topography, and so on (Dirmeyer et al., 2006; Mu et al., 2007; Yuan et al., 2010).

In situ measurements using weighing lysimeter, Bowen ratio, sap flow meters, and eddy covariance technique are generally considered to be reliable for quantifying ET at point and landscape scales (Z. L. Li et al., 2009; Wang and Dickinson, 2012). However, it is practically impossible to apply such methods for quantifying ET at regional and global scales. Fortunately, remote sensing technique which is able to capture temporally continuous land surface information over large areas, provides an effective tool for retrieving the ground parameters which control ET (Ju et al., 2010; Yang et al., 2012). These remotely sensed surface parameters, such as leaf area index (LAI), land cover, clumping index, albedo, temperature, and emissivity, have been successfully used to estimate ET directly or to drive process based models for calculating ET (Yuan et al., 2010; Ryu et al., 2011).

Various models have been developed for estimating ET using remotely sensed data in recent decades (Lu and Zhuang, 2010; Jia et al., 2012), including surface energy balance models (one-source and two-source models) (Jiang and Islam, 1999; Su, 2002; Miralles et al., 2011; Anderson et al., 2012), empirical statistical models (Wang and Liang, 2008), physical models (Penman–Monteith formula) (Mu et al., 2007; K. Zhang et al., 2010), and water balance models (Cheng et al., 2011; Rodell et al., 2011; Sahoo et al., 2011; Zeng et al., 2012; Y. Q. Zhang et al., 2012). The methods used for calculating ET using remote sensing data have been recently reviewed by Z. L. Li et al. (2009) and Wang and Dickinson (2012).

Currently, ET estimated with remote sensing data is far from satisfactory (Yuan et al., 2010). Model structure, inputs, parameterization schemes, and scaling issues are recognized as the major factors affecting the accuracy of ET estimation based on remote sensing at regional and global scales (El Maayar and Chen, 2006; Yuan et al., 2010; Fernandez-Prieto et al., 2012; Jia et al., 2012). It is indispensable to look for effective

HESSD
10, 5397–5456, 2013

ways to constrain uncertainties in estimating ET using remote sensing data. With the rapid development of remote sensing techniques, improving capacity of computation and storage, and increasing availability of ET measurements in recent years (Mu et al., 2011; Ryu et al., 2011; Sasai et al., 2011), it becomes feasible to improve ET estimation through improving the spatial resolution of inputs and model structure (Ryu et al., 2011; Vinukollu et al., 2011) and optimizing model parameters.

Affected by monsoon, climate in China is diverse and complex, ranging from tropical to cold-temperate and from humid to extremely dry (Mu et al., 2008; Piao et al., 2010, 2011). Severe droughts and floods frequently impact ecosystems (Liu et al., 2008). In the past decade, the global has experienced the most significant increase in temperature since instrumental measurements began (Trenberth et al., 2007; Zhao and Running, 2010). As a sensitive region of the climate system, China also experienced significant increases in mean annual temperature (MAT) and changes in seasonal and interannual patterns of precipitation during the past two decades (Fang et al., 2010; Piao et al., 2011) and was more frequently hit by severe droughts (Gao and Yang, 2009; Piao et al., 2009; Qin et al., 2010; Lu et al., 2011; Wang et al., 2011). Climate change and corresponding impacts on the terrestrial water cycle have been becoming a major challenge with which China have to cope (Piao et al., 2010).

The terrestrial water cycle is also significantly affected by land cover change, which has been dramatically occurring in China. For environment protection and vegetation restoration, several large-scale forest plantations programs have been implemented by Chinese government since the late 1970s (Cao et al., 2011; Yu et al., 2011; Huang et al., 2012; Piao et al., 2012), resulting in the increase of forested area during the period from 2000 to 2010 (FAO, 2010) (Piao et al., 2012). Meanwhile, urbanization has been dramatically occurring in China (Li et al., 2011; J. Y. Liu et al., 2012; Wang et al., 2012). The human intervention interacted with climate changes would inevitably alter the terrestrial water cycle in China (Piao et al., 2007).

In recent years, several studies have been conducted to quantify the spatial-temporal variations of ET in China with different methods, such as estimating national and

HESSD
10, 5397–5456, 2013

regional ET using pan evaporation observations and remote sensing driven ecosystem models (M. L. Liu et al., 2008, 2012; Zhou et al., 2009; Zhu et al., 2010). However, most of national ET calculations were implemented at relatively coarse resolutions (i.e. 10 km) and did not fully make use of remote sensing data. In addition, the changes of water yield in the terrestrial ecosystems of China have been less studied. This suggests that more thorough investigation of ET and water yield incorporating land surface information retrieved from remote sensing should be carried out for better understanding how the terrestrial water cycle in China has responded to recent changes in climate and vegetations.

In this study, the process-based Boreal Ecosystem Productivity Simulator (BEPS) model was employed to study the variations of ET and water yield over China during the period from 2000 to 2010 through improving ET calculation with a newly developed LAI dataset. Prior to the regional simulation, the BEPS model was validated with ET measured using the eddy covariance technique at 5 typical ChinaFLUX sites and ET inferred using statistical hydrological data in 10 basins across China. Then, the spatial and temporal variations of ET and water yield and underlying driving factors were examined. The main objectives of this study are: (1) to evaluate the ability of the BEPS model to simulate ET in different ecosystems of China at site and basin scales; (2) to analyze the spatial and temporal patterns of ET and water yield in China's terrestrial ecosystems during the period from 2000 to 2010; (3) to assess the roles of temperature, precipitation, and LAI in regulating ET.

2 Methods and data used

2.1 The model used

The tool used in this study is the BEPS model (Liu et al., 1997), which was originally stemmed from the FOREST-BGC model (Running and Coughlan, 1988). This model includes a two-leaf (sunlit and shaded leaves) photosynthesis module for calculating

HESSD
10, 5397–5456, 2013

carbon fixation, an energy balance and hydrological module for simulating ET and soil water content dynamics, and a soil biogeochemical module for simulating soil heterotrophic respiration and soil carbon and nitrogen dynamics. The photosynthesis module was developed on the basis of Farquhar's instantaneous leaf biochemical model (Farquhar et al., 1980) with a new spatial and temporal scaling scheme (Chen et al., 1999) to calculate daily carbon fixation by the canopy. Although initially developed to calculate net primary productivity for boreal ecosystems in Canada, this model has been improved in many aspects and successfully applied to estimate regional terrestrial water and carbon fluxes in China (Sun et al., 2004; Wang et al., 2005; Feng et al., 2007; Zhou et al., 2009; Ju et al., 2010; Liu et al., 2013), East Asia (Matsushita and Tamura, 2002; F. Zhang et al., 2010; F. Zhang et al., 2012b), North America (Liu et al., 1999; Ju et al., 2006; Sonnentag et al., 2008; Sprintsin et al., 2012; F. Zhang et al., 2012a), Europe (Wang et al., 2004), and the global (Chen et al., 2012).

Since the details about the BPES model were described in (Liu et al., 1997, 2003; Chen et al., 1999, 2005; Ju et al., 2006), only some main methodologies and recent modifications directly related to the calculation of ET are provided here.

2.1.1 ET calculation

In the BEPS model, ET from terrestrial ecosystems is calculated as:

$$ET = T_r + E_{plant} + S_{plant} + E_{soil} + S_{ground} \quad (1)$$

where T_r is the transpiration from the canopy; E_{plant} and E_{soil} are the evaporation of intercepted precipitation and soil surface, respectively; S_{plant} and S_{ground} are the snow sublimation from the canopy and ground surface, respectively.

The transpiration from the canopy is further calculated as:

$$T_r = T_{r,sun} LAI_{sun} + T_{r,shaded} LAI_{shaded} \quad (2)$$

where $T_{r,sun}$ and $T_{r,shaded}$ are the transpiration from the sunlit and shaded leaves, respectively; LAI_{sun} and LAI_{shaded} represent the LAI of the sunlit and shaded leaves,

HESSD
10, 5397–5456, 2013

respectively and they are partitioned according to total LAI of the canopy, daily mean solar zenith angle (θ), and clumping index (Ω) (Chen et al., 1999).

The transpiration of sunlit and shaded leaves are calculated using the Penman–Monteith equation (Monteith, 1965):

$$T_{r,j} = \frac{\Delta R_{n,j} + \rho c_p \mathrm{VPD}/r_a}{(\Delta + r(1 + r_{s,j}/r_a))\lambda v} \quad (3)$$

where Δ is the rate of saturated water vapor pressure changing with temperature ($\mathrm{kPa\,^{\circ}C^{-1}}$); the subscript j denotes the sunlit or shaded leaves; $R_{n,j}$ is the net radiation ($\mathrm{w\,m^{-2}}$) absorbed by sunlit or shaded leaves; ρ is the density of air ($\mathrm{kg\,m^{-3}}$); c_p is the specific heat of air ($\mathrm{J\,kg^{-1}\,^{\circ}C^{-1}}$); γ is the psychrometric constant ($\mathrm{kPa\,^{\circ}C^{-1}}$); r_a is the aerodynamic resistance ($\mathrm{s\,m^{-1}}$); $r_{s,j}$ is the stomatal resistance to water vapor ($\mathrm{s\,m^{-1}}$) of sunlit or shaded leaves.

E_{soil} is also calculated using the Penman–Monteith equation with the resistance of soil surface changing with the degree of saturation within the first soil layer (Ju et al., 2010). E_{plant}, S_{plant}, and S_{ground} are computed in the same way as (Liu et al., 2003).

2.1.2 Stomatal resistance calculation

Stomatal resistance of sunlit and shaded leaves is determined using the Jarvis model (Jarvis, 1976), i.e.

$$r_j = r_{min} f(T) f(\mathrm{VPD}) f(\mathrm{PPFD}_j) f(W) \quad (4)$$

where r_{min} is the minimum stomatal resistance ($\mathrm{s\,m^{-1}}$) depending on land cover types; $f(T)$, $f(\mathrm{VPD})$, $f(\mathrm{PPFD}_j)$, and $f(W)$ are the scalars quantifying the effects of temperature, atmospheric vapor pressure deficit, photosynthetically active radiation, and soil water content on stomatal resistance, respectively.

HESSD
10, 5397–5456, 2013

With the consideration that vegetation is able to optimize the uptake of soil water, soil water scalar f_w in Eq. (4) is determined as:

$$f_w = \sum_{i=1}^{n} f_{w,i}\beta_i \tag{5}$$

where $f_{w,i}$ is the soil water stress factor in layer i; β_i is the weight of layer i expressed as a function of soil water availability and root abundance (Ju et al., 2006):

$$\beta_i = \frac{r_i f_{w,i}}{\sum_{i=1}^{n} r_i f_{w,i}} \tag{6}$$

where r_i is the root fraction within layer i and determined following (Zhang and Wegehenkel, 2006).

In Eq. (6), the term $f_{w,i}$ in layer i is calculated as (Chen et al., 2005; Ju et al., 2010):

$$f_{w,i} = \begin{cases} \max\left[0.25, 2\left(\frac{\theta_i-\theta_{w,i}}{\theta_{f,i}-\theta_{w,i}}\right) - \left(\frac{\theta_i-\theta_{w,i}}{\theta_{f,i}-\theta_{w,i}}\right)^2\right] & \theta_i \le \theta_{f,i} \\ 1 - 0.4\left(\frac{\theta_i-\theta_{f,i}}{\theta_{s,i}-\theta_{f,i}}\right) & \theta_i > \theta_{f,i} \end{cases} \tag{7}$$

where θ_i is the simulated volumetric soil water content; $\theta_{w,i}$, $\theta_{f,i}$ and $\theta_{s,i}$ are the wilting point, field capacity, and porosity of soil layer i, respectively. They are determined according to the fractions of clay, silt, and sand (Saxton et al., 1986).

2.1.3 Soil water content simulation

Originally, BEPS used a bucket model approach to simulate soil water content (Liu et al., 2003). In this study, the soil profile was stratified into three layers with thicknesses of 0.1, 0.25, and 0.85 m, respectively. Soil evaporation is limited to the first soil layer while vegetations can uptake water from all three layers through transpiration.

HESSD
10, 5397–5456, 2013

Therefore, the changes of soil water content in three soil layers can be simulated as:

$$\frac{\partial \theta_1}{\partial t} = \frac{1}{d_1}\left[P_{gs} - T_{r,1} - E_s - RF - Q_{1,2}\right] \quad (8a)$$

$$\frac{\partial \theta_2}{\partial t} = \frac{1}{d_2}\left[Q_{1,2} - T_{r,2} - Q_{2,3}\right] \quad (8b)$$

$$\frac{\partial \theta_3}{\partial t} = \frac{1}{d_3}\left[Q_{2,3} - T_{r,3} - Q_3\right] \quad (8c)$$

where θ_i is the water content of soil layer i; d_i is the thickness of soil layer i (m); P_{gs} is precipitation throughfall arriving the ground surface ($m\,d^{-1}$); $T_{r,i}$ is the transpiration uptake from soil layer i ($m\,d^{-1}$); E_s is the evaporation loss from the soil surface ($m\,d^{-1}$); RF is the surface runoff estimated as a function of P_{gs} and θ_1; $Q_{i,i+1}$ is the vertical exchange of soil water between adjacent soil layers i and $(i+1)$ ($m\,d^{-1}$); and Q_3 is the saturated subsurface flow from the bottom of soil profile and calculated according to soil water content and saturated hydraulic conductivity in the deepest soil layer.

The flux of soil water between adjacent layers i and $(i+1)$ is simulated as (Sellers et al., 1996):

$$Q_{i,i+1} = \frac{k_i d_i + k_{i+1} d_{i+1}}{d_i + d_{i+1}}\left(1 + 2\frac{w_i - w_{i+1}}{d_i + d_{i+1}}\right) \quad (9)$$

where k_i and k_{i+1} are the hydraulic conductivity ($m\,d^{-1}$) in soil layers i and $i+1$, respectively; w_i and w_{i+1} are the water potential (m) in layers i and $i+1$, respectively.

The hydraulic conductivity of soil layer i is calculated as:

$$k_i = K_i\left(\frac{\theta_i}{\theta_{s,i}}\right)^{2b+3} \quad (10)$$

HESSD
10, 5397–5456, 2013

where K_i is the saturated hydrological conductivity of soil layer i ($m\,d^{-1}$); and b is a parameter determining the rate of hydraulic conductivity changing with soil water content, depending on soil texture.

2.2 Model input data

The BEPS model uses both spatially distributed and static datasets as inputs. Atmospheric CO_2 concentration is assumed well mixed and spatially homogenous. The spatially distributed inputs into the BEPS include: (1) land cover types, (2) LAI time series, (3) daily meteorological data (maximum temperature, minimum temperature, precipitation, incoming short-wave radiation, and relative humidity), and (4) soil texture. Prior to the regional simulation, all spatially explicit input datasets were projected into an Albers conical equal area projection system at a spatial resolution of 500 m × 500 m.

2.2.1 LAI data

The dataset of 8 day LAI at a spatial resolution of 500 m for the period from 2000 to 2010 was generated using an inversion algorithm based on the 4-scale geometrical optical model (Deng et al., 2006). This LAI inversion algorithm was driven by the MODIS Land Cover (MCD12Q1 V051) (Friedl et al., 2010) and reflectance (MOD09A1 V05) products. It inverses LAI based on the relationships between LAI and vegetation indices simulated using the 4-scale geometrical optical model (Chen and Leblanc, 1997) and corrects the effects of changes in sun and sensor angles on reflectance and vegetation indices. Due to its superiority to the MODIS LAI algorithm, which has been proved in Canada, China, and other regions (Liu et al., 2007; Pisek et al., 2007; X. Li et al., 2009; Y. Liu et al., 2012), this LAI inversion algorithm was already adopted by the GLOBCARBON project supported by European Space Agency to generate the global LAI product. The inversed LAI was further smoothed using the Locally Adjusted Cubic-spline Capping (LACC) method (Chen et al., 2006) to remove unrealistic fluctuations caused by residual cloud contamination and atmospheric noises.

HESSD
10, 5397–5456, 2013

2.2.2 Land cover data

The annual MODIS land cover data set (MCD12Q1 V051) at a spatial resolution of 500 m (Friedl et al., 2010) from 2001 to 2010 was used to assign plant physiological parameters required in the LAI inversion algorithm and BEPS model. Owing to the deficiency of MODIS land cover data in 2000, the MODIS land cover dataset in 2001 was used as a surrogate of that in 2000. In comparison with the Collection 4 land cover data (Friedl et al., 2002), the Collection 5 land cover data has been substantially improved in spatial resolution and classification algorithm (Friedl et al., 2010). This MODIS land cover product was generated using a regression tree method in combination with MODIS reflectance of band 1 to 7, albedo, land-surface temperature, texture, and so on (Friedl et al., 2002, 2010). In the MCD12Q1 V051 product, there are 5 different land cover datasets corresponding to different classification systems. In this study, the dataset generated using the IGBP land cover classification system (Loveland and Belward, 1997) was used and further aggregated into 10 vegetation cover type groups, including evergreen needleleaf forest (ENF), evergreen broadleaf forest (EBF), deciduous needleleaf forest (DNF), deciduous broadleaf forest (DBF), mixed forest (MF), shrubland (SH), grassland (GRA), cropland (CRO), cropland/Natural vegetation mosaic (NAV), and Non-vegetation (NOV) (Fig. 1).

2.2.3 Meteorological data

The daily meteorological data, including maximum and minimum temperatures, relative humidity, sunshine duration, and precipitation observed at 753 national basic meteorological stations in China (Fig. 2) was used to generate 500 m meteorological fields for the period from 2000 to 2010 using the inverse distance weighted interpolation method. Since incoming solar radiation required by the BEPS model is only observed at 102 meteorological stations in China, it was calculated using observed daily sunshine duration in this study. In the interpolation of temperatures, a lapse rate of 6 °C per 1000 m was assumed. There is no observed meteorological data available in Taiwan province

HESSD
10, 5397–5456, 2013

and meteorological stations in northwestern China, such as Xinjiang, Qinghai-Tibetan Plateau, are sparse (Fig. 2). The limited meteorological observations in these areas would inevitably induce uncertainties in interpolated meteorological data and consequently in simulated ET and water yield.

2.2.4 Soil data

The soil texture spatial maps generated using the 1 : 1 000 000 scale soil map of China and 8595 soil profiles recorded in the second national soil survey dataset developed by Shangguan et al. (2012) were also interpolated to a spatial resolution of 500 m to drive the BEPS model. The soil texture, represented by the volumetric percentages of clay, sand, and silt components, was used to estimate hydrological parameters, including the wilting point (water potential at 1500 kPa), field capacity (water potential at 33 kPa), porosity, saturated hydrological conductivity, air entry water potential, and so on.

2.3 Model validation

In previous studies, the performance of the BEPS model to simulate ET flux has been validated by using measurements in North America (Liu et al., 2003), East Asia (F. Zhang et al., 2010), and China (Wang et al., 2005). In this study, it was further evaluated using ET measured with the eddy-covariance (EC) technique at 5 typical sites of ChinaFLUX and basin-level ET inferred from statistical precipitation and run off data in 10 basins across China.

2.3.1 ET measured using the EC technique

The simulated ET was compared with EC measurements at 5 typical sites of ChinaFLUX (Yu et al., 2006), including the Changbaishan temperate broad-leaved Korean pine mixed forest (CBS) site, Qianyanzhou subtropical coniferous plantation site (QYZ), Haibei alpine meadow site (HB), Xilinhot temperate steppe site (XLHT), and Yucheng warmer temperate cropland site (YC) (Fig. 2). Detailed information about these 5 sites

HESSD
10, 5397–5456, 2013

is listed in Table 1. ET measured in every 30 min was aggregated into daily values (named observed ET hereafter) for model validation.

2.3.2 ET inferred from statistical hydrological data in 10 basins

ET calculated by the BEPS model was further validated at basin scales. According to basin depiction on the hydrological yearbook of China, the mainland China was divided into 10 major river basins, namely Songhua river basin (SHRB), Liaohe river basin (LRB), Haihe river basin (HaiRB), Yellow river basin (YeRB), Huaihe river basin (HuaiRB), Yangtze river basin (YzRB), Southeast river basin (SERB), Pearl river basin (PRB), Southwest river basin (SWRB), and Northwest river basin (NWRB) (Fig. 2).

The statistical data of annual precipitation and run off during the period from 2000 to 2010 was collected from "China Water Resources Bulletin" (The Ministry of Water Resources of the People's Republic of China, http://www.mwr.gov.cn/zwzc/hygb/szygb/). Prior to 2003, SHRB and LRB were lumped together as one basin named as Song-Liao basin on the Bulletin. So, statistical hydrological data in SHRB and LRB was only available after 2003. With the assumption that the annual change in total water storage within a basin is negligible (Liu et al., 2008; Zhang et al., 2009; Vinukollu et al., 2011), basin-level annual ET was calculated as the residual of precipitation minus runoff (named as inferred basin-level ET hereafter).

2.4 Accuracy assessment and trend analysis

Three metrics including coefficient of determination (R^2), absolute predictive error (APE), and relative predictive error (RPE) were used to evaluate the performance of the BEPS model in simulating ET. APE and RPE are calculated as:

$$\mathrm{APE} = \mathrm{ETs} - \mathrm{ETo} \tag{11}$$

$$\mathrm{RPE} = \left[(\mathrm{ETs} - \mathrm{ETo})/\mathrm{ETo}\right] \times 100\,\% \tag{12}$$

where ETs and ETo are the simulated and observed annual ET, respectively.

HESSD
10, 5397–5456, 2013

The linear fitting method ($y = ax + b$) was used to analyze the temporal trends of hydrological variables (ET and water yield), mean annual temperature (MAT), annual precipitation, and annual mean LAI during the period from 2000 to 2010:

$$a = \left[n \sum_{i=1}^{n} x_i y_i - \sum_{i=1}^{n} x_i \sum_{i=1}^{n} y_i \right] / \left[n \sum_{i=1}^{n} x_i^2 - \left(\sum_{i=1}^{n} x_i \right)^2 \right] \quad (13)$$

where n is the number of years (equal to 11 in this study); x_i denotes the year (= 1, 2, 3, . . . , 11); y_i represents the annual mean or total of a variable in the ith year. A positive a value means an increasing trend, and vice versa.

3 Results and discussion

3.1 BEPS model evaluation

3.1.1 Comparison of simulated ET with EC measurements

Figure 3 shows the seasonal variations of simulated and observed daily ET at 5 typical ChinaFLUX sites. Overall, BEPS was able to capture the seasonality of ET well. However, it tended to overestimate daily ET in autumn at the YC cropland site and underestimate that in spring at the HB grassland site. The regression line between simulated and observed daily ET was very close to 1 : 1 line at all sites, with slopes ranging from 0.84 to 1.05 and intercepts lower than 0.10 (Table 2). The R^2 of simulated daily ET against observations was mostly above 0.60 at 5 sites. However, the BEPS model performed relatively poor in simulating ET at the YC site, with R^2 equal to 0.61 and 0.44 in 2003 and 2004, respectively. When data at 5 sites lumped together, the BEPS model explained about 66 % of the variation of daily ET ($p < 0.0001$) (Fig. 4).

At annual scales, simulated ET matched observations well (Table 2). RPE of simulated annual ET was in the range of ±10 % at the CBS, QYZ, XLHT, and YC (Fig. 4,

HESSD
10, 5397–5456, 2013

Table 2) sites. However, RPE was −27.73 % at the HB site in 2003, mainly due to the underestimation of ET in spring.

3.1.2 Validation of simulated basin-level annual ET

Figure 5 shows the comparison of simulated annual ET with basin-level ET inferred using the water balance method in 10 basins (Fig. 2) for the period from 2000 to 2010. The basin-level annual ET simulated by the BEPS model matched with the inferred basin-level ET well. The BEPS model could explain 92 % of the variations of inferred basin-level ET among different basins and years ($p < 0.0001$). However, the differences between annual basin-level ET simulated by the BEPS model and inferred ones are relatively large in HaiRB, HuaiRB, PRB, and SERB (Fig. 5a). Averaged over the 11 yr study period, simulated basin-level annual ET was slightly lower than the inferred values in YeRB, HuaiRB, and HaiRB. The underestimation of simulated ET in these regions might be attributed to the exclusion of irrigation in the BEPS model. Croplands are widely distributed in YeRB, HuaiRB, and HaiRB. Irrigation is a popular management practice in these regions. It greatly alleviates water stress and enhances stomatal conductance and in turn ET. Without consideration of irrigation in the BEPS model would result in the overestimation of soil water stress and consequently the underestimation of ET in croplands of these regions. In SHRB and LRB in northeastern China, ET simulated by the BEPS model is higher than that the inferred using the water balance method (Fig. 5b). These regions are normally covered by deep snowpack in winter and early spring. The uncertainties in estimation of snow sublimation here might result in the overestimation of annual ET. In addition, precipitation was interpolated from measurements at limited meteorological stations and the horizontal redistribution of soil water is not considered in this study. These shortcomings could definitely cause the disagreement between simulated ET and the estimates using the water balance method.

HESSD
10, 5397–5456, 2013

3.2 Spatial patterns of simulated ET and water yield

3.2.1 Spatial patterns of simulated annual ET

Figure 6a shows the spatial patterns of simulated ET in terrestrial ecosystems of China averaged over the period from 2000 to 2010. There were obviously identical spatial variations in mean annual ET relating to climate and vegetation types, with a decreasing trend from the southeast to the northwest. The spatial patterns of ET identified here are consistent with the findings in the previous studies (Liu et al., 2008; Zhou et al., 2009). Overall, ET was high in regions with tropical evergreen forests widely distributed, such as PRB and SERB (Fig. 2). It was low in NWRB of Northwestern China. Mean annual ET in YzRB, HuaiRB, PRB and SERB was normally above 500 mm yr^{-1}. In PRB and SERB, mean annul ET was even above 700 mm yr^{-1}. Within YzRB, ET showed an increasing trend from the upstream to downstream areas. It ranged from 200 to 400 mm yr^{-1} in the upstream areas (such as southern Qinghai province and eastern Sichuan province), from 500 to 700 mm yr^{-1} in the middle stream areas, and even more than 700 mm yr^{-1} in the downstream regions. In SWRB, mean annual ET exhibited significant heterogeneity, lower than 150 mm yr^{-1} in western Tibet, ranging from 200 to 300 mm yr^{-1} in central Tibet, from 600 to 800 mm yr^{-1} in southeastern Tibet and southern Yunnan province.

In northern China, mean annual ET showed an obviously decreasing pattern from the east to the west. In SHRB and LRB, mean annual ET was about 600 mm yr^{-1} in forest areas and 300 mm yr^{-1} in cropland and grassland areas. Similar linkage of ET with land cover types also occurred in YeRB. In HaiRB dominantly covered by croplands, mean annual ET was around 500 mm yr^{-1}. In arid NWRB, mean annual ET was normally less than 150 mm yr^{-1} due to limited water supply and sparse vegetation.

Averaged over the basin scale, ET was the highest in PRB (729 mm yr^{-1}), followed by that in SERB (714 mm yr^{-1}), HuaiRB (568 mm yr^{-1}), and YzRB (552 mm yr^{-1}). Average ET was the lowest in NWRB (144 mm yr^{-1}) and followed by that in YeRB (349 mm yr^{-1}).

HESSD
10, 5397–5456, 2013

The totals of ET within individual basins ranged from 106.28 $km^3 yr^{-1}$ (in LRB) to 986.79 $km^3 yr^{-1}$ (in YzRB) (Fig. 7).

The national mean of simulated annual ET in China's landmass was 369.8 $mm yr^{-1}$ for the period from 2000 to 2010, which is comparable with the global values reported in some previous studies. Dirmeyer et al. (2006) indicated that the global means of annual ET ranged from 272 to 441 $mm yr^{-1}$ based on the simulations of 15 models in the Global Soil Wetness Project-2. However, mean ET in China simulated in this study was lower than some recently reported global values. Fisher et al. (2008) indicated that the global mean of ET equaled 444 $mm yr^{-1}$ during the period from 1986 to 1993 estimated using the Priestley–Taylor model driven by the AVHRR remote sensing data. Yuan et al. (2010) pointed out that global mean ET was 417 ± 38 $mm yr^{-1}$ across the vegetated area during the period from 2000 to 2003. Much higher global means of ET were also reported by Ryu et al. (2011) (500 ± 104 $mm yr^{-1}$), K. Zhang et al. (2010) (539 ± 9 $mm yr^{-1}$), Jung et al. (2010) (550 $mm yr^{-1}$) and Zeng et al. (2012) (604 $mm yr^{-1}$). In a synthesis study, Mueller et al. (2011) declared that the means of global ET ranged from 544 $mm yr^{-1}$ to 631 $mm yr^{-1}$, depending on which types of models were used. Therefore, it can be concluded that the mean of ET in the terrestrial ecosystems of China simulated in this study is somewhat lower than the global value due to the vast semiarid and arid regions in northwestern and northern China and the vast frigid Tibetan Plateau, in which ET is very low (Fig. 6a).

The total of ET in terrestrial ecosystems of China varied from 3.26 to 3.65×10^3 km^3 with a mean of 3.49×10^3 km^3 during the period from 2000 to 2010, which accounted for about 5 % of the global total of 58.4×10^3 $km^3 yr^{-1}$ (Yan et al., 2012), 63×10^3 $km^3 yr^{-1}$ (Ryu et al., 2011), 65×10^3 $km^3 yr^{-1}$ (Jung et al., 2010), 65.5×10^3 $km^3 yr^{-1}$ (Oki and Kanae, 2006).

HESSD
10, 5397–5456, 2013

3.2.2 Spatial patterns of simulated annual water yield

Water yield is calculated as the difference between annual precipitation and ET (M. L. Liu et al., 2012). It showed a very similar spatial pattern to ET and was above zero in most areas of China's territory (Fig. 6b). However, in arid NWRB, insufficient precipitation is unable to meet the requirement of ET, resulting in slightly negative water yield. In southern basins, precipitation was higher than ET, resulting in significantly positive water yield. For example, water yield was widely above 600 $mm\,yr^{-1}$ in PRB and SERB, even above 1000 $mm\,yr^{-1}$ in southeastern coastal areas. In vast YzRB, it ranged from 100 $mm\,yr^{-1}$ in the upstream to 800 $mm\,yr^{-1}$ in the downstream. Water yield was usually about 100 $mm\,yr^{-1}$ in most regions of SHRB, eastern LRB, HaiRB, and the upstream of YeRB.

3.2.3 Dependence of simulated ET on land cover types

The simulated ET is closely associated with land cover types. Figure 8 shows the average of simulated annual ET for each land cover type during the period from 2000 to 2010. The EBF biome has the largest average ET (885.5 $mm\,yr^{-1}$), followed by MF (653.3 $mm\,yr^{-1}$), ENF (624.0 $mm\,yr^{-1}$), NAV (600.5 $mm\,yr^{-1}$), DBF (518.1 $mm\,yr^{-1}$), CRO (498.3 $mm\,yr^{-1}$), DNF (345.4 $mm\,yr^{-1}$), GRA (280.7 $mm\,yr^{-1}$), and SH (200.1 $mm\,yr^{-1}$). The non-vegetation cover type, widely distributed in northwest China, has the lowest mean ET (113.6 $mm\,yr^{-1}$). MF has the highest total annual ET (834.70 $km^3\,yr^{-1}$), followed by GRA (808.60 $km^3\,yr^{-1}$), and CRO (796.27 $km^3\,yr^{-1}$) due to the large area of these three land cover types. Although the mean ET of EBF is the highest, the total ET of this land cover type only ranked as the seventh because of its relative small area. The totals of annual ET were less than 50 $km^3\,yr^{-1}$ for DNF, DBF, and SH, owing to low mean ET per unit area or small areas of these land cover types.

The change of simulated ET with land cover types in China identified here is generally consistent with previous studies (Liu et al., 2008; Zhou et al., 2009; K. Zhang

HESSD
10, 5397–5456, 2013

et al., 2010; Jin et al., 2011), showing that ET of forests is higher than that of cropland and grassland. However, ET of ENF and MF simulated in this study is significantly higher than the global values reported by K. Zhang et al. (2010). Recently, M. L. Liu et al. (2012) simulated that average ET over eastern China was 567 mm yr^{-1} during the period from 2001 to 2005, about 10 % higher than the corresponding value output by the BEPS model here.

3.3 Temporal trends of ET and water yield in terrestrial ecosystems of China

3.3.1 Temporal trends of ET

Figure 9 shows the temporal trends of simulated annual ET in terrestrial ecosystems of China during the period from 2000 to 2010. ET increased in 62.2 % of China's landmass. The greatest increase of ET occurred in the cropland areas of southern HaiRB, most HuaiRB, and southeastern YzRB, with increasing rates above 10 mm yr^{-2}. Annual ET increased at rates of 6 to 10 mm yr^{-2} in northern HuaiRB and the forest areas of western SHRB, YeRB, and YzRB. The increase rates of annual ET were small, only about 2 mm yr^{-2} in NWRB, such as Inner Mongolia, Qinghai-Tibet plateau. On the other hand, annual ET decreased in eastern SHRB, northwestern NWRB, southern SWRB, and southern PRB. In eastern Qinghai-Tibetan plateau, the south part of Yunnan province, and Hainan province, the decrease in ET was most significant, at rates of above 8 mm yr^{-2}.

Figure 10 shows the departures of simulated annual ET from 11 yr means in 10 basins. Annual ET increased in all basins but NWRB. The increases of mean annual ET in HuaiRB, YzRB, and SWRB were above the 0.1 significant levels. Mean annual ET in YeRB, SHRB, SERB, HaiRB, PRB, and LRB showed a relatively slight increase trend. In years 2000 to 2002, especially in 2001, mean annual ET in all basins was lower than the multi-year averages. In contrast, mean annual ET over the period from 2004 to 2008 was mostly above the multi-year averages in all basins. In 2009, ET obviously decreased in all basins except SERB. In NWRB, ET in this year even decreased by

HESSD
10, 5397–5456, 2013

15 % in comparison with the multi-year mean. In 2003 and 2010, changes of ET relative to multi-year means varied spatially, increasing in the northern basins and decreasing in the southern basins.

The trends of ET during the period from 2000 to 2010 in southern China (Figs. 9 and 10) identified in this study are consistent with the result reported by Jung et al. (2010) for the period from 1998 to 2008. Both studies indicated decreasing trends of ET in PRB and southern SERB and increasing trends of ET in vast YzRB and southern HuaiRB. Recently, Zeng et al. (2012) studied the spatial-temporal changes of global land ET for the period from 1982 to 2009 using a land water mass balance equation and found out that annual ET increased in HuaiRB and HaiRB and decreased in PRB during the period from 1998 to 2009. Similar temporal patterns of ET in these areas were also detected in this study for the period from 2000 to 2010. However, the opposite temporal trends of ET were found in two studies for both YzRB and SERB. Zeng et al. (2012) indicated that ET decreased in these two basins while the increased ET was detected in this study.

National means of annual ET varied from 345.5 $mm\,yr^{-1}$ in 2001 to 387.8 $mm\,yr^{-1}$ in 2005, with an average of 369.8 $mm\,yr^{-1}$ over the period from 2000 to 2010 (Fig. 10). It exhibited an overall increasing trend in terrestrial ecosystems of China during the studied period, with an increasing rate of 1.7 $mm\,yr^{-2}$ ($r = 0.43$ $p = 0.19$). National mean ET increased in years from 2001 to 2005 and then gradually decreased to the second lowest value of 361.6 $mm\,yr^{-1}$ in 2009. In the period from 2004 to 2008, the national mean of ET land was above the multi-year average (369.8 $mm\,yr^{-1}$). The obvious decrease of national ET in 2001 and 2009 was caused by the wide occurrence of severe droughts.

3.3.2 Temporal trends of water yield

Figure 12 shows temporal trends of water yield in terrestrial ecosystems of China during the period from 2000 to 2010, which exhibited substantial spatial heterogeneity. Water yield decreased in northern, southern, southwestern, and central China, while

HESSD
10, 5397–5456, 2013

it increased in northwestern, northeastern, and eastern China. In NWRB and HaiRB, water yield changed slightly, at a magnitude of ±4 mm yr^{-2}. The significant increase in water yield mainly occurred in southeastern SHRB, eastern LRB, and downstream areas of YzRB, with rates of about 20 mm yr^{-2}. YeRB experienced a moderate decrease in water yield (about 8 mm yr^{-2}) during the 11 yr study period. Water yield decreased obviously in HuaiRB, SWRB, southern YzRB, and western PRB, at rates even above 20 mm yr^{-2} in some areas.

The temporal trends of ET and water yield indentified in this study imply that the terrestrial hydrological cycle was intensified in most regions of China in recent 11 yr, indicating by the significant increase in ET in most areas. Consequently, the availability of water resources was affected. In most regions south of Yangtze River and HuaiRB, enhanced ET in conjunction with decrease in precipitation has caused water yield to decrease significantly.

3.4 Linkage of ET with climate factors

ET is affected by a variety of factors, including water availability, energy supply, wind speed, vapor pressure deficit (VPD), and vegetation activity (Zhang et al., 2001; Verstraeten et al., 2008; Wang and Dickinson, 2012). It is still a challenge to identify drivers for regional ET. In analyzing the roles of climate factors in ET, temperature is often used as the surrogate of radiation and VPD due to their strong correlations (Jung et al., 2010; Zeng et al., 2012). Here annual precipitation (as the proxy of water availability) and MAT (as the proxy of available energy) were chosen to explore the effects of climate variability on the spatial and temporal variations of ET in China's landmass for the period from 2000 to 2010.

Figure 13a and c shows the temporal trends of annual precipitation and MAT during the past 11 yr. Precipitation decreased significantly in southern China, such as HuaiRB, south YzRB, SWRB, and PRB. In some parts of these regions, the decreasing rates of annual precipitation were even above 24 mm yr^{-1}. Meanwhile, temperature increased by above 0.04 °C yr^{-1}, even more than 0.1 °C yr^{-1} in the upstream areas of YzRB and

HESSD
10, 5397–5456, 2013

SWRB. In northern China, MAT did not increase obviously while precipitation increased by 5–10 mm yr^{-1}. The decrease in precipitation and increase in temperature were induced by several severe drought events in southern China during the period from 2000 to 2010 (Gao and Yang, 2009; Lu et al., 2011; Wang et al., 2011).

Figure 13b and d shows the correlation coefficients of annual ET with annual total precipitation and MAT during the period from 2000 to 2010, respectively. Annual ET was positively correlated with annual precipitation in most regions of China, especially in the arid and semiarid regions of northern China, such as NWRB, western SHRB, western LRB, and HaiRB, in which the positive correlations between ET and precipitation was above the 0.01 significant level. The obvious increase of above 8 mm yr^{-2} in annual ET in HaiRB, western SHRB, and the upstream of YeRB (Fig. 9) can be partially explained by the significant increase in annual precipitation in these regions (> 6 mm yr^{-1}). In humid southeastern China and the frigid Tibetan plateau, annual ET and precipitation were negatively correlated at the 0.10 and 0.05 significant levels, respectively. In these regions, water supply is relatively sufficient. The increase in precipitation is normally accompanied with the reduction in temperature and incoming solar radiation, and consequently the decease of ET.

Annual ET increased with the increase in MAT in the Qinghai-Tibetan plateau, PRB, most YzRB and YeRB, and HuaiRB (Fig. 13d). In the Qinghai-Tibetan plateau, especially in southeastern NWRB, most SWRB, the upstream areas of YeRB and YzRB, the positive correlations of ET with MAT were above the 0.05 significant level. In these regions, temperature acts as the major limiting factor of ET. The obvious increase of about 0.1 °C yr^{-1} here (Fig. 13c) was the main driver for the increase of above 4 mm yr^{-2} in annual ET (Fig. 9). On the contrary, in most NWRB, HuaiRB, SHRB, LRB, central YzRB, central YeRB, and southern SERB, annual ET was negatively correlated with MAT ($p < 0.1$).

Figure 14 shows the changes in the departures of annual ET from multi-year means with the departures of annual total precipitation and MAT in individual basins. The basin-level average annual ET showed much stronger dependence on precipitation

HESSD
10, 5397–5456, 2013

in northern basins than in southern basins. In SHRB, LRB, HaiRB, YeRB, and NWRB, the departures of annual ET were positively correlated with those of precipitation. The correlations were above the 0.05 significance level in SHRB and LRB and above the 0.01 significance level in HaiRB and NWRB, respectively. Changes in precipitation did not have significant impact on ET in humid southern regions of China. The changes of annual precipitation and annual ET were slightly negative correlated in SERB, PRB, and SWRB. Basin-level average ET was not significantly correlated with basin-level averages of MAT in all basins.

Several previous studies have investigated the controlling roles of different climate factors in ET of terrestrial ecosystems in China. Zhou et al. (2009) pointed out that precipitation plays a more important role in altering the inter-annual variations of annual ET over China than temperature. Cong et al. (2010) concluded that precipitation had a greater impact on ET in the north than in the south. In the study on the linkages of global ET with MAT and precipitation during the period from 1982 to 2008, Jung et al. (2010) declared that precipitation (water supply) dominated the inter-annual ET behavior in northern China while in southern China ET was mainly demand (temperature) limited. Using daily meteorological data and gauging station data, Q. Zhang et al. (2011) indicated that precipitation was the major determinate of ET in YeRB. Since in the semiarid and arid northern areas of China, ET was limited by the supply of soil moisture, precipitation significantly affected soil moisture and acted as a key constraining factor of ET here (Ryu et al., 2008; Wang and Dickinson, 2012). The impacts of temperature and precipitation on ET in different regions identified here are generally similar to the conclusions from previous studies, but with more details due to a higher spatial resolution of simulation (500 m) conducted and proper applications of remote sensing data here.

HESSD
10, 5397–5456, 2013

3.5 Influences of vegetation on ET

3.5.1 Changes of ET with LAI

LAI significantly affects ET due to its roles in transpiration and interception of precipitation. During the period from 2000 to 2010, annual mean LAI increased in northeastern, northern, and most south central China while it decreased in southeastern and parts of southwestern China (Fig. 15a). Similar conclusions on vegetation greenness in China during the same period were also recently reported by Liu and Gong (2012). The spatial heterogeneity in the temporal trends of LAI and greenness were mainly associated with climatic abnormality and land cover changes (Peng et al., 2011; Y. Liu et al., 2012).

During the 11 yr study period, simulated annual ET was positively correlated with annual mean LAI in 74 % of China's landmass (Fig. 15a). The correlation between LAI and ET was stronger in the north than in the south. In most of SHRB, LRB, HaiRB, HuaiRB, and YeRB as well as part of YzRB, annual ET increased significantly ($p < 0.05$) with the increase of LAI. Thus, the obvious increase of above 8 mm yr^{-2} in annual ET in HaiRB, HuaiRB, and central YzRB can be partially explained by the significant increase in annual mean LAI here ($> 0.03\,yr^{-1}$). Annual ET was slightly positively correlated with annual mean LAI in most regions south of the Yangtze River, such as SERB, southern YzRB, and PRB. The distinguishable decrease in annual ET in southern China, such as southern Qinghai-Tibet Plateau, the junction area of YzRB, SWRB, and PRB, and eastern PRB might be caused by the significant decrease in annual mean LAI here. In most NWRB, vegetation coverage is relatively low and thus evaporation from soil is the dominant component of ET. The increase in LAI might cause the increase in transpiration and more decrease in soil evaporation. As a consequence, the correlation of ET with LAI was slightly negative here.

HESSD
10, 5397–5456, 2013

3.5.2 The influences of land cover change on ET

ET is closely linked with land cover types. Model simulation and site observations showed that ET of forests was generally higher than that of croplands and grasslands (Zhang et al., 2001; Liu et al., 2008; Mu et al., 2011). Land cover changes have been dynamically occurring in China, driven by afforestation/reforestation and urbanization, inevitably leading to increases in plantation and urban areas and decreases in croplands and grasslands areas (Li et al., 2011; Wang et al., 2012). In order to assess the effect of land cover changes on regional ET, the means of ET and changing rates of mean ET, total ET, and areas of forests (including ENF, EBF, DNF, DBF, and MF), cropland, and grassland were calculated in 10 basins and listed in Table 3. During the period from 2000 to 2010, these three land cover types totally accounted for 67.8 % to 70.5 % and 83.4 % to 86.3 % of the national totals of area and ET, respectively.

National wide mean ET of forests, cropland, and grassland in China increased during the study period (Table 3). The mean ET of cropland showed the largest increase ($2.38\,mm\,yr^{-2}$), followed by that of forest and grassland. As to forest, mean ET increased in most basins except LRB, SWRB, and NWRB. The mean ET of cropland and grassland increased in northern basins and decreased in southern basins. In PRB, mean ET of cropland and grassland decreased at the rates of $3.37\,mm\,yr^{-2}$ ($p = 0.06$) and $9.76\,mm\ yr^{-2}$ ($p = 0.0016$), respectively. The national total ET of forest, cropland, and grassland all increased during the period from 2000 to 2010. The total ET of forests increased significantly in 7 basins, resulting in the national total ET of forests to increase at a rate of $13.35\,km^3\,yr^{-2}$ ($p = 0.0015$). The increase in the national total ET of forests was driven by the increases in both mean ET and the area. The expansion of forest area played a more dominant role. During the past 11 yr, the national total of forest area increased at a rate of $1.79 \times 10^6 ha\,yr^{-2}$ ($p = 0.0026$). The national total ET of cropland increased at the rate of $2.83\,km^3\,yr^{-2}$, mainly driven by the increase in the mean of ET since the national total area of cropland decreased at a rate of $0.99 \times 10^6\,ha\,yr^{-1}$. The total ET of cropland only increased in HaiRB, YeRB, HuaiRB,

HESSD
10, 5397–5456, 2013

and SERB, and decreased in other 6 basins. The national total ET on grassland increased at the rate of 1.25 $km^3 yr^{-2}$, driven by the increases in both mean ET and the area. Total ET of grassland increased in most northern basins and decreased in most southern basins except SWRB. The decrease in total ET of grassland in southern basins was caused by the decreases in both mean ET and the area. In HuaiRB and PRB, total ET of grassland significantly decreased at the rates of 0.43 $km^3 yr^{-2}$ ($p = 0.006$) and 0.80 $km^3 yr^{-2}$ ($p = 0.0017$), respectively.

During the period from 2000 to 2010, the total ET of terrestrial ecosystems in China increased at a rate of 14.29 $km^3 yr^{-2}$. This increase might be mainly attributed to the increase in total ET of forests (13.35 $km^3 yr^{-2}$). Our simulation showed that ET of forests (except DNF) was obviously higher than that of other land cover types (Fig. 8), which was similar to the findings of previous studies (Twine et al., 2004; Sun et al., 2005, 2006; Yu et al., 2009; Q. Zhang et al., 2011). They reported that the conversion from crop and grass to forest can cause annual ET to increase and water yield to decrease, vice versa. Sun et al. (2006) indicated that the average water yield reduction caused by land cover conversion was about 50 $mm yr^{-1}$ (50 %) in the semiarid Loess Plateau region in northern China to about 300 $mm yr^{-1}$ (30 %) in the tropical southern region. With simulations of a hydrological model, Yu et al. (2009) declared that changing grassland into forest caused a significant reduction of water yield and an increase of ET in a watershed of the Liupan Mountains in northwest China. Based on daily meteorological and gauging stations data, Q. Zhang et al. (2011) found out that the intensifying urbanization acted as one important factor to the decrease of ET in the PRB.

4 Conclusions

In this study, the BEPS model was employed in conjunction with the newly developed dataset of LAI to simulate ET and water yield in China at a spatial resolution of 500 m for the period from 2000 to 2010. The ability of BEPS to simulate ET was firstly validated using tower-based ET at 5 ChinaFLUX sites and basin-level ET inferred using statistical

HESSD
10, 5397–5456, 2013

hydrological data in 10 major river basins. Then, the spatial and temporal variations of ET and water yield and the influences of climatic and vegetation factors were analyzed. Following conclusions could be drawn:

(1) The BEPS model was able to simulate ET in China's terrestrial ecosystems, explaining 66 % of the variations of observed daily ET at 5 typical ChinaFLUX sites. The RPE values of simulated annual ET were mostly in the ±10 % ranges of the observed values. The BEPS model could explain the 92 % variations of inferred basin-level ET in 10 river basins ($p < 0.0001$).

(2) Simulated mean annual ET exhibited a distinguishable decreasing spatial pattern from southeast to the northwest, associating with climate and vegetation types. The averages of simulated mean annual ET ranged from 200.1 $mm\,yr^{-1}$ for shrubland to 885.5 $mm\,yr^{-1}$ for evergreen broadleaf forest. Annual ET increased with the increase of LAI in 74 % of China's landmass, especially in SHRB, LRB, HaiRB, HuaiRB, and YeRB. It was positively correlated with temperature in most areas of southwest, south, east, and central China, especially in the Tibet Plateau and part of the middle stream of the Yangtze River. In the arid and semiarid areas of northwest and north China, annual ET was significantly positively correlated with annual precipitation while in the Tibet Plateau and humid southeast China, the correlation between precipitation and ET was negative.

(3) The national mean annual ET averaged 369.8 $mm\,yr^{-1}$ during the period from 2000 to 2010, ranging from 345.5 $mm\,yr^{-1}$ in 2001 to 387.8 $mm\,yr^{-1}$ in 2005. It increased at a rate of 1.7 $mm\,yr^{-2}$ ($r = 0.43$ $p = 0.19$), mainly driven by the increase of ET in forests. National total ET increased during the period from 2001 to 2005 and decreased during the period from 2006 to 2009. The decrease of national total ET during the second period was mainly caused by the reductions of precipitation and LAI. The temporal trends of annual ET varied spatially. In 62.2 % of China's terrestrial ecosystems, ET showed increasing trends, especially in the cropland areas of southern HaiRB, most HuaiRB, and southeastern YzRB. The decrease of annual ET mainly occurred in part areas of northeast, north, northwest, south China. In eastern

HESSD
10, 5397–5456, 2013

Qinghai-Tibet plateau, the south part of Yunnan province, and Hainan province, the decrease in ET was most significant, at rates above 8 mm yr^{-2}.

(4) Water yield was above zero in most China's terrestrial ecosystems, especially in southeast and south regions. However, it was negative in most areas of NWRB in northwest China. During the study period, water yield decreased in northern, southern, and southwestern China. In some areas, water yield even decreased at rates above 20 mm yr^{-2} caused by enhanced ET and decrease in precipitation, implying that climatic variability and vegetation changes have significantly intensified terrestrial hydrological cycle and reduced water resource here. The regions with water yield increase were sporadically distributed in northeast, east, south, northwest, and central China, in which precipitation increased or/and ET decreased.

The conclusions are very useful for studying the coupling between carbon and water cycles and also managing water resources efficiently in China. However, it should be kept in mind that there are still some uncertainties in this study. Although most of spatial datasets driving the model were taken from ground observations and remote sensing data, some uncertainties may exist in these datasets, such as limited meteorological observations available and errors in remotely sensed vegetation parameters. Model validation was only implemented at limited sites and basins. In addition, the shortcomings in the structure of the BEPS model, such as the application of Jarvis model for calculating canopy conductance and exclusion of irrigation and lateral movement of soil water in the calculation of soil water content, might cause some errors in estimated ET and water yield. All these deficiencies need to be addressed carefully in the future.

Acknowledgements. This research was supported by National Basic Research Program of China (2010CB833503 and 2010CB950702), Chinese Academy of Sciences (XDA05050602-1), and the Priority Academic Program Development of Jiangsu Higher Education Institutions (PAPD). The authors would greatly thank Qiuan Zhu (Northwest A&F University) for providing the digital boundary of river basins in China.

HESSD
10, 5397–5456, 2013

References

Anderson, R. G., Jin, Y., and Goulden, M. L.: Assessing regional evapotranspiration and water balance across a Mediterranean montane climate gradient, Agr. Forest Meteorol., 166–167, 10–22, doi:10.1016/j.agrformet.2012.07.004, 2012.

Cao, S. X., Chen, L., Shankman, D., Wang, C. M., Wang, X. B., and Zhang, H.: Excessive reliance on afforestation in China's arid and semi-arid regions: lessons in ecological restoration, Earth-Sci. Rev., 104, 240–245, doi:10.1016/j.earscirev.2010.11.002, 2011.

Chen, J. M. and Leblanc, S. G.: A four-scale bidirectional reflectance model based on canopy architecture, IEEE T. Geosci. Remote, 35, 1316–1337, 1997.

Chen, J. M., Liu, J., Cihlar, J., and Goulden, M. L.: Daily canopy photosynthesis model through temporal and spatial scaling for remote sensing applications, Ecol. Model., 124, 99–119, 1999.

Chen, J. M., Chen, X. Y., Ju, W. M., and Geng, X. Y.: Distributed hydrological model for mapping evapotranspiration using remote sensing inputs, J. Hydrol., 305, 15–39, 2005.

Chen, J. M., Deng, F., and Chen, M. Z.: Locally adjusted cubic-spline capping for reconstructing seasonal trajectories of a satellite-derived surface parameter, IEEE T. Geosci. Remote, 44, 2230–2238, 2006.

Chen, J. M., Mo, G., Pisek, J., Liu, J., Deng, F., Ishizawa, M., and Chan, D.: Effects of foliage clumping on the estimation of global terrestrial gross primary productivity, Global Biogeochem. Cy., 26, GB1019, doi:10.1029/2010gb003996, 2012.

Cheng, L., Xu, Z., Wang, D., and Cai, X.: Assessing interannual variability of evapotranspiration at the catchment scale using satellite-based evapotranspiration data sets, Water Resour. Res., 47, W09509, doi:10.1029/2011wr010636, 2011.

Cong, Z. T., Zhao, J. J., Yang, D. W., and Ni, G. H.: Understanding the hydrological trends of river basins in China, J. Hydrol., 388, 350–356, doi:10.1016/j.jhydrol.2010.05.013, 2010.

Deng, F., Chen, J. M., Plummer, S., Chen, M. Z., and Pisek, J.: Algorithm for global leaf area index retrieval using satellite imagery, IEEE T. Geosci. Remote, 44, 2219–2229, doi:10.1109/tgrs.2006.872100, 2006.

Dirmeyer, P. A., Gao, X., Zhao, M., Guo, Z., Oki, T., and Hanasaki, N.: GSWP-2: Multimodel analysis and implications for our perception of the land surface, B. Am. Meteorol. Soc., 87, 1381–1397, doi:10.1175/bams-87-10-1381, 2006.

HESSD
10, 5397–5456, 2013

El Maayar, M. and Chen, J. M.: Spatial scaling of evapotranspiration as affected by heterogeneities in vegetation, topography, and soil texture, Remote Sens. Environ., 102, 33–51, 2006.
Fang, J., Tang, Y., and Son, Y.: Why are East Asian ecosystems important for carbon cycle research?, Sci. China Life Sci., 53, 753–756, doi:10.1007/s11427-010-4032-2, 2010.
FAO: Food and Agriculture Organization: Global Forest Resources Assessment, Rome, Italy, 2010.
Farquhar, G. D., Caemmerer, S. V., and Berry, J. A.: A biochemical-model of photosynthetic CO_2 assimilation in leaves of C_3 species, Planta, 149, 78–90, 1980.
Feng, X., Liu, G., Chen, J. M., Chen, M., Liu, J., Ju, W. M., Sun, R., and Zhou, W.: Net primary productivity of China's terrestrial ecosystems from a process model driven by remote sensing, J. Environ. Manage., 85, 563–573, doi:10.1016/j.jenvman.2006.09.021, 2007.
Fernandez-Prieto, D., van Oevelen, P., Su, Z., and Wagner, W.: Advances in Earth observation for water cycle science, Hydrol. Earth Syst. Sci., 16, 543–549, doi:10.5194/hess-16-543-2012, 2012.
Fisher, J. B., Tu, K. P., and Baldocchi, D. D.: Global estimates of the land-atmosphere water flux based on monthly AVHRR and ISLSCP-II data, validated at 16 FLUXNET sites, Remote Sens. Environ., 112, 901–919, 2008.
Fisher, J. B., Whittaker, R. J., and Malhi, Y.: ET come home: potential evapotranspiration in geographical ecology, Global. Ecol. Biogeogr., 20, 1–18, doi:10.1111/j.1466-8238.2010.00578.x, 2011.
Friedl, M. A., McIver, D. K., Hodges, J. C. F., Zhang, X. Y., Muchoney, D., Strahler, A. H., Woodcock, C. E., Gopal, S., Schneider, A., Cooper, A., Baccini, A., Gao, F., and Schaaf, C.: Global land cover mapping from MODIS: algorithms and early results, Remote Sens. Environ., 83, 287–302, Pii s0034-4257(02)00078-0doi:10.1016/s0034-4257(02)00078-0, 2002.
Friedl, M. A., Sulla-Menashe, D., Tan, B., Schneider, A., Ramankutty, N., Sibley, A., and Huang, X.: MODIS collection 5 global land cover: algorithm refinements and characterization of new datasets, Remote Sens. Environ., 114, 168–182, doi:10.1016/j.rse.2009.08.016, 2010.
Gao, H. and Yang, S.: A severe drought event in northern China in winter 2008–2009 and the possible influences of La Nina and Tibetan Plateau, J. Geophys. Res.-Atmos., 114, 2009.

HESSD
10, 5397–5456, 2013

Huang, L., Liu, J., Shao, Q., and Xu, X.: Carbon sequestration by forestation across China: Past, present, and future, Renew. Sust. Energ. Rev., 16, 1291–1299, doi:10.1016/j.rser.2011.10.004, 2012.

Huntington, T. G.: Evidence for intensification of the global water cycle: Review and synthesis, J. Hydrol., 319, 83–95, 2006.

Hutjes, R. W. A., Kabat, P., Running, S. W., Shuttleworth, W. J., Field, C., Bass, B., Dias, M., Avissar, R., Becker, A., Claussen, M., Dolman, A. J., Feddes, R. A., Fosberg, M., Fukushima, Y., Gash, J. H. C., Guenni, L., Hoff, H., Jarvis, P. G., Kayane, I., Krenke, A. N., Liu, C., Meybeck, M., Nobre, C. A., Oyebande, L., Pitman, A., Pielke, R. A., Raupach, M., Saugier, B., Schulze, E. D., Sellers, P. J., Tenhunen, J. D., Valentini, R., Victoria, R. L., and Vorosmarty, C. J.: Biospheric aspects of the hydrological cycle – Preface, J. Hydrol., 212, 1–21, doi:10.1016/s0022-1694(98)00255-8, 1998.

Jarvis, P. G.: The Interpretation of Variations in Leaf Water Potential and Stomatal Conductance Found in Canopies in Field, Philos. T. Roy. Soc. B, 273, 593–610, 1976.

Jia, Z., Liu, S., Xu, Z., Chen, Y., and Zhu, M.: Validation of remotely sensed evapotranspiration over the Hai River Basin, China, J. Geophys. Res.-Atmos., 117, D13113, doi:10.1029/2011jd017037, 2012.

Jiang, L. and Islam, S.: A methodology for estimation of surface evapotranspiration over large areas using remote sensing observations, Geophys. Res. Lett., 26, 2773–2776, doi:10.1029/1999gl006049, 1999.

Jin, Y., Randerson, J. T., and Goulden, M. L.: Continental-scale net radiation and evapotranspiration estimated using MODIS satellite observations, Remote Sens. Environ., 115, 2302–2319, doi:10.1016/j.rse.2011.04.031, 2011.

Ju, W. M., Chen, J. M., Black, T. A., Barr, A. G., Liu, J., and Chen, B. Z.: Modelling multi-year coupled carbon and water fluxes in a boreal aspen forest, Agr. Forest Meteorol., 140, 136–151, 2006.

Ju, W. M., Gao, P., Wang, J., Zhou, Y. L., and Zhang, X. H.: Combining an ecological model with remote sensing and GIS techniques to monitor soil water content of croplands with a monsoon climate, Agr. Water Manage., 97, 1221–1231, 2010.

Jung, M., Reichstein, M., Ciais, P., Seneviratne, S. I., Sheffield, J., Goulden, M. L., Bonan, G., Cescatti, A., Chen, J., de Jeu, R., Dolman, A. J., Eugster, W., Gerten, D., Gianelle, D., Gobron, N., Heinke, J., Kimball, J., Law, B. E., Montagnani, L., Mu, Q., Mueller, B., Oleson, K., Papale, D., Richardson, A. D., Roupsard, O., Running, S., Tomelleri, E., Viovy, N.,

HESSD
10, 5397–5456, 2013

Weber, U., Williams, C., Wood, E., Zaehle, S., and Zhang, K.: Recent decline in the global land evapotranspiration trend due to limited moisture supply, Nature, 467, 951–954, doi:10.1038/nature09396, 2010.

Koster, R. D., Dirmeyer, P. A., Guo, Z. C., Bonan, G., Chan, E., Cox, P., Gordon, C. T., Kanae, S., Kowalczyk, E., Lawrence, D., Liu, P., Lu, C. H., Malyshev, S., McAvaney, B., Mitchell, K., Mocko, D., Oki, T., Oleson, K., Pitman, A., Sud, Y. C., Taylor, C. M., Verseghy, D., Vasic, R., Xue, Y. K., Yamada, T., and Team, G.: Regions of strong coupling between soil moisture and precipitation, Science, 305, 1138–1140, 2004.

Li, J., Yu, Q., Sun, X., Tong, X., Ren, C., Wang, J., Liu, E., Zhu, Z., and Yu, G.: Carbon dioxide exchange and the mechanism of environmental control in a farmland ecosystem in North China Plain, Sci. China Ser. D, 49, 226–240, doi:10.1007/s11430-006-8226-1, 2006.

Li, X., Ju, W., Zhou, Y., and Chen, S.: Retrieving leaf area index of forests in red soil hilly region using remote sensing data, Second International Conference on Earth Observation for Global Changes (EOGC 2009): Remote Sensing of Earth Surface Changes, Chengdu, China, 74710–74719, 2009.

Li, Z., Yu, G., Xiao, X., Li, Y., Zhao, X., Ren, C., Zhang, L., and Fu, Y.: Modeling gross primary production of alpine ecosystems in the Tibetan Plateau using MODIS images and climate data, Remote Sens. Environ., 107, 510–519, doi:10.1016/j.rse.2006.10.003, 2007.

Li, Z., Gao, Z., Gao, W., Shi, R., and Liu, C.: Spatio-temporal feature of land use/land cover dynamic changes in China from 1999 to 2009, Transactions of the Chinese Society of Agricultural Engineering, 27, 312–322, 2011.

Li, Z. L., Tang, R., Wan, Z., Bi, Y., Zhou, C., Tang, B., Yan, G., and Zhang, X.: A review of current methodologies for regional evapotranspiration estimation from remotely sensed data, Sensors-Basel, 9, 3801–3853, doi:10.3390/s90503801, 2009.

Li, Z. Q., Yu, G. R., Wen, X. F., Zhang, L. M., Ren, C. Y., and Fu, Y. L.: Energy balance closure at ChinaFLUX sites, Sci. China Ser. D, 48, 51–62, 2005.

Liu, J., Chen, J. M., Cihlar, J., and Park, W. M.: A process-based boreal ecosystem productivity simulator using remote sensing inputs, Remote Sens. Environ., 62, 158–175, 1997.

Liu, J., Chen, J. M., Cihlar, J., and Chen, W.: Net primary productivity distribution in the BOREAS region from a process model using satellite and surface data, J. Geophys. Res.-Atmos., 104, 27735–27754, 1999.

HESSD
10, 5397–5456, 2013

Liu, J., Chen, J. M., and Cihlar, J.: Mapping evapotranspiration based on remote sensing: An application to Canada's landmass, Water Resour. Res., 39, 1189, doi:10.1029/2002WR001680, 2003.
Liu, J. Y., Zhang, Q., and Hu, Y. F.: Regional differences of China's urban expansion from late 20th to early 21st century based on remote sensing information, Chinese Geogr. Sci., 22, 1–14, doi:10.1007/s11769-012-0510-8, 2012.
Liu, M. L., Tian, H. Q., Chen, G. S., Ren, W., Zhang, C., and Liu, J. Y.: Effects of land-use and land-cover change on evapotranspiration and water yield in China during 1900–2000, J. Am. Water Resour. Assoc., 44, 1193–1207, doi:10.1111/j.1752-1688.2008.00243.x, 2008.
Liu, M. L., Tian, H. Q., Lu, C. Q., Xu, X. F., Chen, G. S., and Ren, W.: Effects of multiple environment stresses on evapotranspiration and runoff over eastern China, J. Hydrol., 426, 39–54, doi:10.1016/j.jhydrol.2012.01.009, 2012.
Liu, R., Chen, J. M., Liu, J., Deng, F., and Sun, R.: Application of a new leaf area index algorithm to China's landmass using MODIS data for carbon cycle research, J. Environ. Manage., 85, 649–658, 2007.
Liu, S. and Gong, P.: Change of surface cover greenness in China between 2000 and 2010, Chinese Sci. Bull., 57, 2835–2845, doi:10.1007/s11434-012-5267-z, 2012.
Liu, Y., Yu, G., Wen, X., Wang, Y., Song, X., Li, J., Sun, X., Yang, F., Chen, Y., and Liu, Q.: Seasonal dynamics of CO_2 fluxes from subtropical plantation coniferous ecosystem, Sci. China Ser. D, 49, 99–109, doi:10.1007/s11430-006-8099-3, 2006.
Liu, Y., Ju, W., Chen, J., Zhu, G., Xing, B., Zhu, J., and He, M.: Spatial and temporal variations of forest LAI in China during 2000–2010, Chinese Sci. Bull., 57, 2846–2856, doi:10.1007/s11434-012-5064-8, 2012.
Liu, Y., Ju, W., He, H., Wang, S., Sun, R., and Zhang, Y.: Changes of net primary productivity in China during recent 11 years detected using an ecological model driven by MODIS data, Frontiers of Earth Science, 7, 112–127, doi:10.1007/s11707-012-0348-5, 2013.
Loveland, T. R. and Belward, A. S.: The IGBP-DIS global 1 km land cover data set, DISCover: First results, Int. J. Remote Sens., 18, 3289–3295, doi:10.1080/014311697217099, 1997.
Lu, E., Luo, Y., Zhang, R., Wu, Q., and Liu, L.: Regional atmospheric anomalies responsible for the 2009–2010 severe drought in China, J. Geophys. Res.-Atmos., 116, D21114, doi:10.1029/2011jd015706, 2011.

HESSD
10, 5397–5456, 2013

Lu, X. L. and Zhuang, Q. L.: Evaluating evapotranspiration and water-use efficiency of terrestrial ecosystems in the conterminous United States using MODIS and AmeriFlux data, Remote Sens. Environ., 114, 1924–1939, 2010.
Matsushita, B. and Tamura, M.: Integrating remotely sensed data with an ecosystem model to estimate net primary productivity in East Asia, Remote Sens. Environ., 81, 58–66, 2002.
Meehl, G. A. and Tebaldi, C.: More intense, more frequent, and longer lasting heat waves in the 21st century, Science, 305, 994–997, doi:10.1126/science.1098704, 2004.
Miralles, D. G., Holmes, T. R. H., De Jeu, R. A. M., Gash, J. H., Meesters, A. G. C. A., and Dolman, A. J.: Global land-surface evaporation estimated from satellite-based observations, Hydrol. Earth Syst. Sci., 15, 453–469, doi:10.5194/hess-15-453-2011, 2011.
Monteith, J. L.: Evaporation and the environment, Proceedings of the Symposium on Experimental Biology, 19, 205–234, 1965.
Mu, Q., Heinsch, F. A., Zhao, M., and Running, S. W.: Development of a global evapotranspiration algorithm based on MODIS and global meteorology data, Remote Sens. Environ., 111, 519–536, 2007.
Mu, Q., Zhao, M., Running, S. W., Liu, M., and Tian, H.: Contribution of increasing CO_2 and climate change to the carbon cycle in China's ecosystems, J. Geophys. Res.-Biogeo., 113, G01018, doi:10.1029/2006jg000316, 2008.
Mu, Q. Z., Zhao, M. S., and Running, S. W.: Improvements to a MODIS global terrestrial evapotranspiration algorithm, Remote Sens. Environ., 115, 1781–1800, 2011.
Mueller, B., Seneviratne, S. I., Jimenez, C., Corti, T., Hirschi, M., Balsamo, G., Ciais, P., Dirmeyer, P., Fisher, J. B., Guo, Z., Jung, M., Maignan, F., McCabe, M. F., Reichle, R., Reichstein, M., Rodell, M., Sheffield, J., Teuling, A. J., Wang, K., Wood, E. F., and Zhang, Y.: Evaluation of global observations-based evapotranspiration datasets and IPCC AR4 simulations, Geophys. Res. Lett., 38, L06402, doi:10.1029/2010gl046230, 2011.
Oki, T. and Kanae, S.: Global hydrological cycles and world water resources, Science, 313, 1068–1072, doi:10.1126/science.1128845, 2006.
Peng, S., Chen, A., Xu, L., Cao, C., Fang, J., Myneni, R. B., Pinzon, J. E., Tucker, C. J., and Piao, S.: Recent change of vegetation growth trend in China, Environ. Res. Lett., 6, 044027, doi:10.1088/1748-9326/6/4/044027, 2011.
Piao, S. L., Friedlingstein, P., Ciais, P., de Noblet-Ducoudre, N., Labat, D., and Zaehle, S.: Changes in climate and land use have a larger direct impact than rising CO_2 on global river

HESSD
10, 5397–5456, 2013

runoff trends, P. Natl. Acad. Sci. USA, 104, 15242–15247, doi:10.1073/pnas.0707213104, 2007.

Piao, S. L., Yin, L., Wang, X. H., Ciais, P., Peng, S. S., Shen, Z. H., and Seneviratne, S. I.: Summer soil moisture regulated by precipitation frequency in China, Environ. Res. Lett., 4, 044012, doi:10.1088/1748-9326/4/4/044012, 2009.

Piao, S. L., Ciais, P., Huang, Y., Shen, Z. H., Peng, S. S., Li, J. S., Zhou, L. P., Liu, H. Y., Ma, Y. C., Ding, Y. H., Friedlingstein, P., Liu, C. Z., Tan, K., Yu, Y. Q., Zhang, T. Y., and Fang, J. Y.: The impacts of climate change on water resources and agriculture in China, Nature, 467, 43–51, 2010.

Piao, S. L., Ciais, P., Lomas, M., Beer, C., Liu, H. Y., Fang, J. Y., Friedlingstein, P., Huang, Y., Muraoka, H., Son, Y. H., and Woodward, I.: Contribution of climate change and rising CO_2 to terrestrial carbon balance in East Asia: a multi-model analysis, Glob. Planet. Change, 75, 133–142, 2011.

Piao, S. L., Ito, A., Li, S. G., Huang, Y., Ciais, P., Wang, X. H., Peng, S. S., Nan, H. J., Zhao, C., Ahlström, A., Andres, R. J., Chevallier, F., Fang, J. Y., Hartmann, J., Huntingford, C., Jeong, S., Levis, S., Levy, P. E., Li, J. S., Lomas, M. R., Mao, J. F., Mayorga, E., Mohammat, A., Muraoka, H., Peng, C. H., Peylin, P., Poulter, B., Shen, Z. H., Shi, X., Sitch, S., Tao, S., Tian, H. Q., Wu, X. P., Xu, M., Yu, G. R., Viovy, N., Zaehle, S., Zeng, N., and Zhu, B.: The carbon budget of terrestrial ecosystems in East Asia over the last two decades, Biogeosciences, 9, 3571–3586, doi:10.5194/bg-9-3571-2012, 2012.

Pisek, J., Chen, J. M., and Deng, F.: Assessment of a global leaf area index product from SPOT-4 VEGETATION data over selected sites in Canada, Can. J. Remote Sens., 33, 341–356, 2007.

Qin, N., Chen, X., Fu, G., Zhai, J., and Xue, X.: Precipitation and temperature trends for the Southwest China: 1960–2007, Hydrol. Process., 24, 3733–3744, doi:10.1002/hyp.7792, 2010.

Rodell, M., McWilliams, E. B., Famiglietti, J. S., Beaudoing, H. K., and Nigro, J.: Estimating evapotranspiration using an observation based terrestrial water budget, Hydrol. Process., 25, 4082–4092, doi:10.1002/hyp.8369, 2011.

Running, S. W. and Coughlan, J. C.: A general model of forest ecosystem processes for regional applications, 1. hydrologic balance, canopy gas exchange and primary production processes, Ecol. Model., 42, 125–154, 1988.

HESSD
10, 5397–5456, 2013

Ryu, Y., Baldocchi, D. D., Ma, S., and Hehn, T.: Interannual variability of evapotranspiration and energy exchange over an annual grassland in California, J. Geophys. Res.-Atmos., 113, D09104, doi:10.1029/2007jd009263, 2008.

Ryu, Y., Baldocchi, D. D., Kobayashi, H., van Ingen, C., Li, J., Black, T. A., Beringer, J., van Gorsel, E., Knohl, A., Law, B. E., and Roupsard, O.: Integration of MODIS land and atmosphere products with a coupled-process model to estimate gross primary productivity and evapotranspiration from 1 km to global scales, Global Biogeochem. Cy., 25, GB4017, doi:10.1029/2011gb004053, 2011.

Sahoo, A. K., Pan, M., Troy, T. J., Vinukollu, R. K., Sheffield, J., and Wood, E. F.: Reconciling the global terrestrial water budget using satellite remote sensing, Remote Sens. Environ., 115, 1850–1865, doi:10.1016/j.rse.2011.03.009, 2011.

Sasai, T., Saigusa, N., Nasahara, K. N., Ito, A., Hashimoto, H., Nemani, R., Hirata, R., Ichii, K., Takagi, K., Saitoh, T. M., Ohta, T., Murakami, K., Yamaguchi, Y., and Oikawa, T.: Satellite-driven estimation of terrestrial carbon flux over Far East Asia with 1-km grid resolution, Remote Sens. Environ., 115, 1758–1771, doi:10.1016/j.rse.2011.03.007, 2011.

Saxton, K. E., Rawls, W. J., Romberger, J. S., and Papendick, R. I.: Estimating generalized soil-water characteristics from Texture, Soil Sci. Soc. Am. J., 50, 1031–1036, 1986.

Sellers, P. J., Randall, D. A., Collatz, G. J., Berry, J. A., Field, C. B., Dazlich, D. A., Zhang, C., Collelo, G. D., and Bounoua, L.: A revised land surface parameterization (SiB2) for atmospheric GCMs, Part I: Model formulation, J. Climate, 9, 676–705, 1996.

Shangguan, W., Dai, Y., Liu, B., Ye, A., and Yuan, H.: A soil particle-size distribution dataset for regional land and climate modelling in China, Geoderma, 171–172, 85–91, doi:10.1016/j.geoderma.2011.01.013, 2012.

Sonnentag, O., Chen, J. M., Roulet, N. T., Ju, W., and Govind, A.: Spatially explicit simulation of peatland hydrology and carbon dioxide exchange: influence of mesoscale topography, J. Geophys. Res.-Biogeo., 113, G02005, doi:10.1029/2007JG000605, 2008.

Sprintsin, M., Chen, J. M., Desai, A., and Gough, C. M.: Evaluation of leaf-to-canopy upscaling methodologies against carbon flux data in North America, J. Geophys. Res.-Biogeo., 117, G01023, doi:10.1029/2010jg001407, 2012.

Su, Z.: The Surface Energy Balance System (SEBS) for estimation of turbulent heat fluxes, Hydrol. Earth Syst. Sci., 6, 85–100, doi:10.5194/hess-6-85-2002, 2002.

HESSD
10, 5397–5456, 2013

Sun, G., McNulty, S. G., Lu, J., Amatya, D. M., Liang, Y., and Kolka, R. K.: Regional annual water yield from forest lands and its response to potential deforestation across the southeastern United States, J. Hydrol., 308, 258–268, doi:10.1016/j.jhydrol.2004.11.021, 2005.

Sun, G., Zhou, G. Y., Zhang, Z. Q., Wei, X. H., McNulty, S. G., and Vose, J. M.: Potential water yield reduction due to forestation across China, J. Hydrol., 328, 548–558, doi:10.1016/j.jhydrol.2005.12.013, 2006.

Sun, R., Chen, J. M., Zhu, Q. J., Zhou, Y. Y., Liu, J., Li, J. T., Liu, S. H., Yan, G. J., and Tang, S. H.: Spatial distribution of net primary productivity and evapotranspiration in Changbaishan Natural Reserve, China, using Landsat ETM+ data, Can. J. Remote Sens., 30, 731–742, 2004.

Trenberth, K., Jones, P., Ambenje, P., Bojariu, R., Easterling, D., Klein, T. A., Parker, D., Rahimzadeh, F., Renwick, J., Rusticucci, M., Soden, B., and Zhai, P.: Observations: Surface and Atmospheric Climate Change, NY, USA0003-0007, 236–336, 2007.

Trenberth, K. E., Fasullo, J. T., and Kiehl, J.: Earth's global energy budget, B. Am. Meteorol. Soc., 90, 311–323, doi:10.1175/2008bams2634.1, 2009.

Twine, T. E., Kucharik, C. J., and Foley, J. A.: Effects of land cover change on the energy and water balance of the Mississippi River basin, J. Hydrometeorol., 5, 640–655, doi:10.1175/1525-7541(2004)005<0640:eolcco>2.0.co;2, 2004.

Verstraeten, W. W., Veroustraete, F., and Feyen, J.: Assessment of evapotranspiration and soil moisture content across different scales of observation, Sensors-Basel, 8, 70–117, doi:10.3390/s8010070, 2008.

Vinukollu, R. K., Wood, E. F., Ferguson, C. R., and Fisher, J. B.: Global estimates of evapotranspiration for climate studies using multi-sensor remote sensing data: evaluation of three process-based approaches, Remote Sens. Environ., 115, 801–823, 2011.

Wang, A. H., Lettenmaier, D. P., and Sheffield, J.: Soil Moisture Drought in China, 1950–2006, J. Climate, 24, 3257–3271, 2011.

Wang, K. and Dickinson, R. E.: A review of global terrestrial evapotranspiration: observation, modeling, climatology, and climatic variability, Rev. Geophys., 50, Rg2005, doi:10.1029/2011rg000373, 2012.

Wang, K. and Liang, S.: An improved method for estimating global evapotranspiration based on satellite determination of surface net radiation, vegetation index, temperature, and soil moisture, J. Hydrometeorol., 9, 712–727, doi:10.1175/2007jhm911.1, 2008.

HESSD
10, 5397–5456, 2013

Wang, L., Li, C., Ying, Q., Cheng, X., Wang, X., Li, X., Hu, L., Liang, L., Yu, L., Huang, H., and Gong, P.: China's urban expansion from 1990 to 2010 determined with satellite remote sensing, Chinese Sci. Bull., 57, 2802–2812, doi:10.1007/s11434-012-5235-7, 2012.

Wang, Q., Tenhunen, J., Falge, E., Bernhofer, C., Granier, A., and Vesala, T.: Simulation and scaling of temporal variation in gross primary production for coniferous and deciduous temperate forests, Glob. Change Biol., 10, 37–51, 2004.

Wang, Q. F., Niu, D., Yu, G. R., Ren, C. Y., Wen, X. F., Chen, J. M., and Ju, W. M.: Simulating the exchanges of carbon dioxide, water vapor and heat over Changbai Mountains temperate broadleaved Korean pine mixed forest ecosystem, Sci. China Ser. D, 48, 148–159, 2005.

Wen, X., Yu, G., Sun, X., Li, Q., Ren, C., and Han, S.: Net water vapour exchange over a mixed needle and broad-leaved forest in Changbai Mountain during autumn, J. Geogr. Sci., 13, 463–468, 2003.

Wen, X. F., Yu, G. R., Sun, X. M., Li, Q. K., Liu, Y. F., Zhang, L. M., Ren, C. Y., Fu, Y. L., and Li, Z. Q.: Soil moisture effect on the temperature dependence of ecosystem respiration in a subtropical Pinus plantation of southeastern China, Agr. Forest Meteorol., 137, 166–175, 2006.

Yan, H., Wang, S. Q., Billesbach, D., Oechel, W., Zhang, J. H., Meyers, T., Martin, T. A., Matamala, R., Baldocchi, D., Bohrer, G., Dragoni, D., and Scott, R.: Global estimation of evapotranspiration using a leaf area index-based surface energy and water balance model, Remote Sens. Environ., 124, 581–595, doi:10.1016/j.rse.2012.06.004, 2012.

Yang, Y., Shang, S., and Jiang, L.: Remote sensing temporal and spatial patterns of evapotranspiration and the responses to water management in a large irrigation district of North China, Agr. Forest Meteorol., 164, 112–122, doi:10.1016/j.agrformet.2012.05.011, 2012.

Yu, D. Y., Shi, P. J., Han, G. Y., Zhu, W. Q., Du, S. Q., and Xun, B.: Forest ecosystem restoration due to a national conservation plan in China, Ecol. Eng., 37, 1387–1397, doi:10.1016/j.ecoleng.2011.03.011, 2011.

Yu, G. R., Wen, X. F., Sun, X. M., Tanner, B. D., Lee, X. H., and Chen, J. Y.: Overview of ChinaFLUX and evaluation of its eddy covariance measurement, Agr. Forest Meteorol., 137, 125–137, 2006.

Yu, P., Krysanova, V., Wang, Y., Xiong, W., Mo, F., Shi, Z., Liu, H., Vetter, T., and Huang, S.: Quantitative estimate of water yield reduction caused by forestation in a water-limited area in northwest China, Geophys. Res. Lett., 36, L02406, doi:10.1029/2008gl036744, 2009.

HESSD
10, 5397–5456, 2013

Yuan, W. P., Liu, S. G., Yu, G. R., Bonnefond, J. M., Chen, J. Q., Davis, K., Desai, A. R., Goldstein, A. H., Gianelle, D., Rossi, F., Suyker, A. E., and Verma, S. B.: Global estimates of evapotranspiration and gross primary production based on MODIS and global meteorology data, Remote Sens. Environ., 114, 1416–1431, doi:10.1016/j.rse.2010.01.022, 2010.

Zeng, Z. Z., Piao, S. L., Lin, X., Yin, G. D., Peng, S. S., Ciais, P., and Myneni, R. B.: Global evapotranspiration over the past three decades: estimation based on the water balance equation combined with empirical models, Environ. Res. Lett., 7, 014026, doi:10.1088/1748-9326/7/1/014026, 2012.

Zhang, F., Ju, W., Chen, J., Wang, S., Yu, G., Li, Y., Han, S., and J, A.: Study on evapotranspiration in East Asia using the BEPS ecological model, Journal of Natural Resources, 25, 1596–1606, 2010.

Zhang, F., Chen, J. M., Chen, J., Gough, C. M., Martin, T. A., and Dragoni, D.: Evaluating spatial and temporal patterns of MODIS GPP over the conterminous US against flux measurements and a process model, Remote Sens. Environ., 124, 717–729, doi:10.1016/j.rse.2012.06.023, 2012a.

Zhang, F., Ju, W., Shen, S., Wang, S., Yu, G., and Han, S.: Variations of terrestrial net primary productivity in East Asia, Terr. Atmos. Ocean. Sci., 23, 425–437, doi:10.3319/tao.2012.03.28.01(a), 2012b.

Zhang, K., Kimball, J. S., Mu, Q. Z., Jones, L. A., Goetz, S. J., and Running, S. W.: Satellite based analysis of northern ET trends and associated changes in the regional water balance from 1983 to 2005, J. Hydrol., 379, 92–110, doi:10.1016/j.jhydrol.2009.09.047, 2009.

Zhang, K., Kimball, J. S., Nemani, R. R., and Running, S. W.: A continuous satellite-derived global record of land surface evapotranspiration from 1983 to 2006, Water Resour. Res., 46, W09522, doi:10.1029/2009wr008800, 2010.

Zhang, L., Dawes, W. R., and Walker, G. R.: Response of mean annual evapotranspiration to vegetation changes at catchment scale, Water Resour. Res., 37, 701–708, doi:10.1029/2000wr900325, 2001.

Zhang, M., Yu, G. R., Zhuang, J., Gentry, R., Fu, Y. L., Sun, X. M., Zhang, L. M., Wen, X. F., Wang, Q. F., Han, S. J., Yan, J. H., Zhang, Y. P., Wang, Y. F., and Li, Y. N.: Effects of cloudiness change on net ecosystem exchange, light use efficiency, and water use efficiency in typical ecosystems of China, Agr. Forest Meteorol., 151, 803–816, 2011.

HESSD
10, 5397–5456, 2013

Zhang, Q., Xu, C.-Y., Chen, Y. D., and Ren, L.: Comparison of evapotranspiration variations between the Yellow River and Pearl River basin, China, Stoch. Env. Res. Risk A, 25, 139–150, doi:10.1007/s00477-010-0428-6, 2011.

Zhang, Y. Q. and Wegehenkel, M.: Integration of MODIS data into a simple model for the spatial distributed simulation of soil water content and evapotranspiration, Remote Sens. Environ., 104, 393–408, 2006.

Zhang, Y. Q., Leuning, R., Chiew, F. H. S., Wang, E. L., Zhang, L., Liu, C. M., Sun, F. B., Peel, M. C., Shen, Y. J., and Jung, M.: Decadal trends in evaporation from global energy and water balances, J. Hydrometeorol., 13, 379–391, doi:10.1175/jhm-d-11-012.1, 2012.

Zhao, M. and Running, S. W.: Drought-induced reduction in global terrestrial net primary production from 2000 through 2009, Science, 329, 940–943, doi:10.1126/science.1192666, 2010.

Zhou, L., Wang, S., Chen, J., Feng, X., Ju, W., and Wu, W.: The spatial-temporal characteristics of evapotranspiration of China's terrestrial ecosystems during 1991–2000, Resour. Sci., 31, 962–972, 2009.

Zhu, Q. A., Jiang, H., Liu, J. X., Wei, X. H., Peng, C. H., Fang, X. Q., Liu, S. R., Zhou, G. M., Yu, S. Q., and Ju, W. M.: Evaluating the spatiotemporal variations of water budget across China over 1951–2006 using IBIS model, Hydrol. Process., 24, 429–445, 2010.

HESSD
10, 5397–5456, 2013

Table 1. The information on 5 ChinaFlux sites at which ET data was used for validating the BEPS model.

Site	CBS	QYZ	HB	XLHT	YC
Location	42°24′ N, 128°06′E	26°44′ N, 115°03′ E	37°40′ N, 101°20′ E	43°33′ N, 116°40′ E	36°49′ N, 116°34′ E
Vegetation	Temperate deciduous broad-leaved and coniferous mixed forest	Typical subtropical monsoon man-planted forest	Alpine meadow	Temperate chinensis steppe	Winter wheat and summer maize
Soil type	Mountain dark brown soil	Typical red earth	Alpine meadow soil	Chernozem soil	Aquox and salt aquox
Elevation (m)	736	100	3293	1189	23
Mean annual temperature (°C)	4.0	17.9	−1.4	−0.4	13.1
Annual precipitation (mm)	695	1485	580	350–450	528
LAI	6.1 (maximum in grown season)	3.6	2.8 (maximum in grown season)	1.5 (maximum in grown season)	
Period	2003–2004	2003–2004	2003	2004	2003–2004
Reference	(Wen et al., 2003) (M. Zhang et al., 2011)	(Liu et al., 2006) (Wen et al., 2006)	(Li et al., 2005) (Li et al., 2007)	(Li et al., 2005) (M. Zhang et al., 2011)	(Li et al., 2006) (Wen et al., 2006)

HESSD
10, 5397–5456, 2013

Table 2. Statistics of simulated and observed daily and annual ET at 5 tower sites.

Site	Year	R^2	RMSE ($mm\,d^{-1}$)	a^*	b^*	Observed ET ($mm\,yr^{-1}$)	Simulated ET ($mm\,yr^{-1}$)	APE ($mm\,yr^{-1}$)	RPE (%)
CBS	2003	0.78	0.70	0.99	0.08	537.8	563.3	25.5	4.74
	2004	0.72	0.80	1.05	0.03	524.4	563.9	39.5	7.53
QYZ	2003	0.63	0.73	0.84	0.32	709.4	716.3	6.9	0.97
	2004	0.70	0.85	1.02	0.13	772.4	837.3	64.9	8.40
HB	2003	0.72	0.74	0.86	0.21	499.1	360.7	−138.4	−27.73
XLHT	2004	0.67	0.63	0.98	0.07	311.1	331.0	19.9	6.40
YC	2003	0.61	0.89	0.99	0.08	541.7	509.5	−32.2	−5.9
	2004	0.44	1.31	0.90	0.28	581.9	628.1	46.2	7.94

*$y = ax + b$, y and x denote simulated and observed ET, respectively.

HESSD
10, 5397–5456, 2013

Table 3. Trends in the means and totals of ET and areas of forest, cropland, and grassland in 10 basins during the period from 2000 to 2010.

	Mean ET ($mm\,yr^{-1}$)				Trend of mean ET ($mm\,yr^{-2}$)				Trend of total ET ($km^3\,yr^{-2}$)				Trend of total area ($10^6\,ha\,yr^{-1}$)		
	All land covers	Forest	Cropland	Grassland	All land covers	Forest	Cropland	Grassland	All land covers	Forest	Cropland	Grassland	Forest	Cropland	Grassland
SHRB	418.9	465.7	410.1	343.3	1.96	0.95	1.95	2.28	1.90	1.52^b	−0.04	0.17	0.27^b	−0.28	−0.02
LRB	389.2	539.0	409.9	344.6	1.28	−3.74	1.62	2.32	0.35	0.29^b	−0.41	0.53	0.066^c	-0.21^b	0.12^a
HaiRB	419.4	483.9	444.0	395.1	3.46	2.60	4.17	2.71	1.13	0.34^b	0.97	0.13	0.09^b	−0.05	0.02
YeRB	349.0	532.7	431.6	315.2	2.11	2.31	1.55	1.46	1.77	0.49^c	1.67^a	−0.05	$\mathbf{0.10}^b$	0.22	-0.26^b
HuaiRB	568.1	638.7	586.2	559.9	5.93^a	5.50	6.70^a	−1.79	1.58^a	0.30^c	1.85^a	-0.43^c	0.04^c	0.02	-0.06^b
YzRB	551.7	652.0	604.9	327.7	3.36	4.24	2.60	−0.30	6.01	9.71^c	−0.59	−1.01	1.11^c	−0.58	-0.28^c
SERB	714.4	771.1	615.9	637.5	3.04	3.43	−0.94	−4.83	0.69	0.90^b	0.09	−0.05	0.05^a	−0.007	−0.002
PRB	729.3	770.5	656.2	677.7	0.97	0.45	-3.37^a	-9.76^c	0.57	−0.21	−0.43	-0.80^c	−0.03	−0.12	-0.08^b
SWRB	381.6	707.4	554.9	246.2	1.16^a	−0.94	−1.0	1.22	0.99^a	0	-0.18^b	0.99^b	0.06	-0.04^b	0.11
NWRB	143.9	234.3	225.2	200.2	−0.20	−1.15	−3.19	−0.31	−0.69	0.02	−0.10	1.76	0.03	0.05	1.0^c
Total	369.8	651.4	498.3	280.7	1.71	1.64	2.38	0.42	14.29	13.35^c	2.83	1.25	1.79^c	−0.99	0.55

[a], [b], and [c] represent the 0.10, 0.05, and 0.01 significance levels, respectively (SHRB, Songhua river basin; LRB, Liaohe river basin; HaiRB, Haihe river basin; YeRB, Yellow river basin; HuaiRB, Huaihe river basin; YzRB, Yangtze river basin; SERB, Southeast river basin; PRB, Pearl river basin; SWRB, Southwest river basin; NWRB, Northwest river basin).

HESSD
10, 5397–5456, 2013

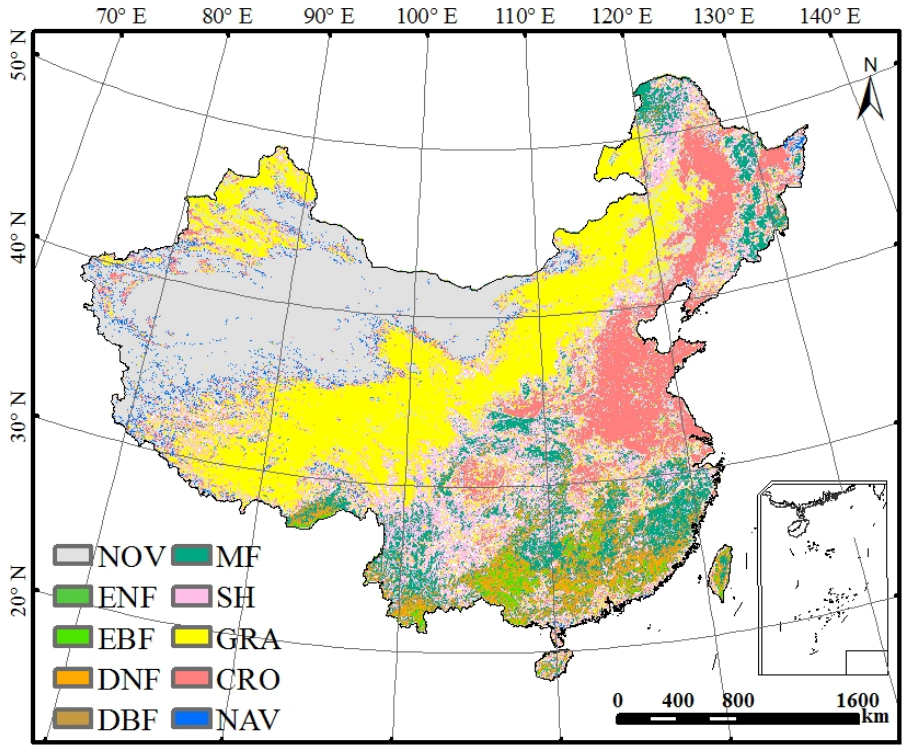

Fig. 1. The land cover map of China in 2001 subtracted from the MODIS land cover dataset. (ENF: evergreen needleleaf forest; EBF: evergreen broadleaf forest; DNF: deciduous needleleaf forest; DBF: deciduous broadleaf forest; MF: mixed forest; SH: shrubland; GRA: grassland; CRO: cropland; NAV: cropland/natural vegetation mosaic; NOV: Non-vegetation).

HESSD
10, 5397–5456, 2013

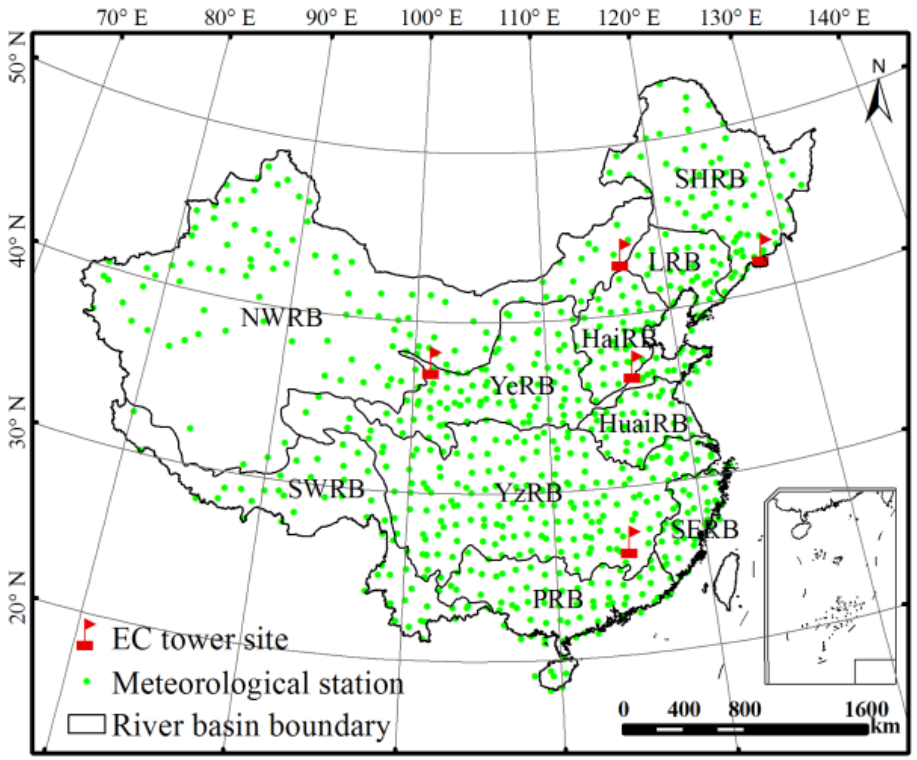

Fig. 2. Locations of the 5 typical flux tower sites (red flags), 753 national basic meteorological stations (green circles), and boundary of 10 river basins (black lines) (SHRB, Songhua river basin; LRB, Liaohe river basin; HaiRB, Haihe river basin; YeRB, Yellow river basin; HuaiRB, Huaihe river basin; YzRB, Yangtze river basin; SERB, Southeast river basin; PRB, Pearl river basin; SWRB, Southwest river basin; NWRB, Northwest river basin).

HESSD
10, 5397–5456, 2013

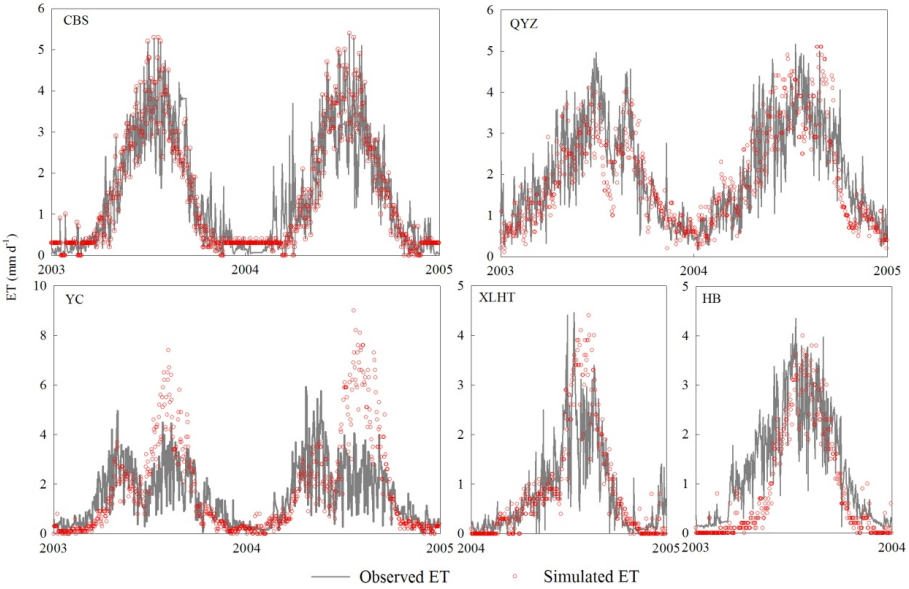

Fig. 3. Time series of observed and simulated daily ET ($mm\,d^{-1}$). during the period of 2003 to 2005 at CBS, QYZ, YC, 2004 to 2005 at XLHT and 2003 to 2004 at HB.

HESSD
10, 5397–5456, 2013

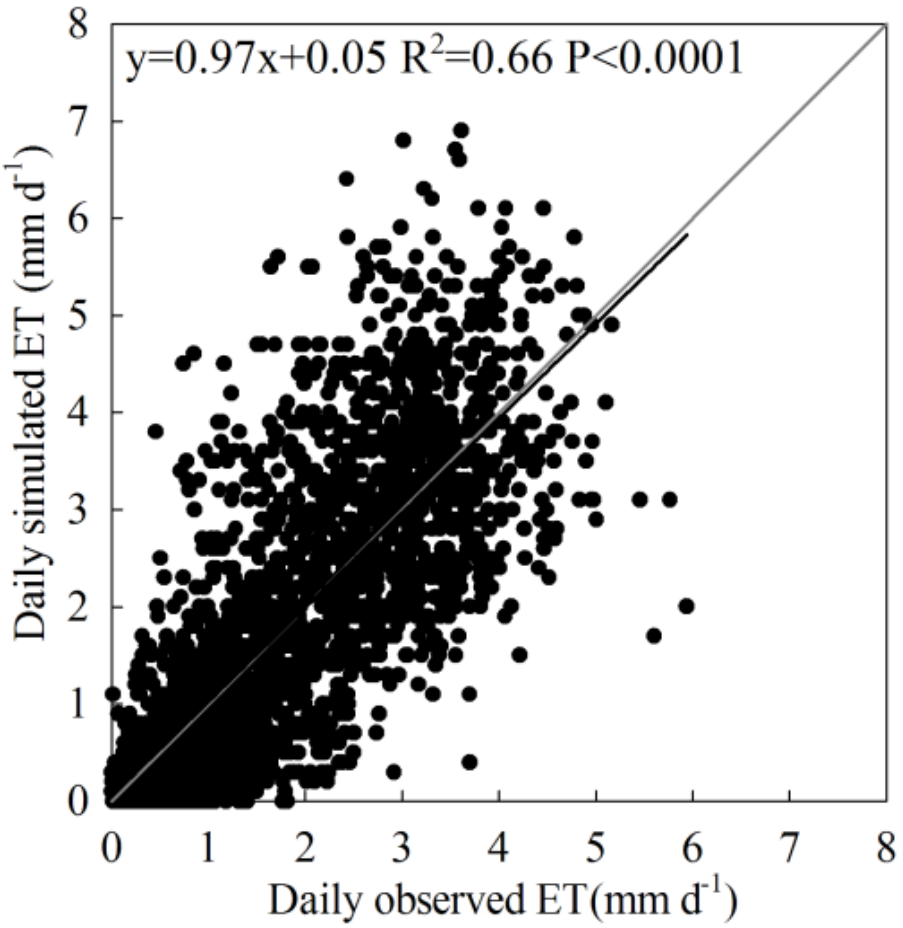

Fig. 4. Comparison between simulated and observed ET (mm d^{-1}) at all 5 tower sites.

HESSD
10, 5397–5456, 2013

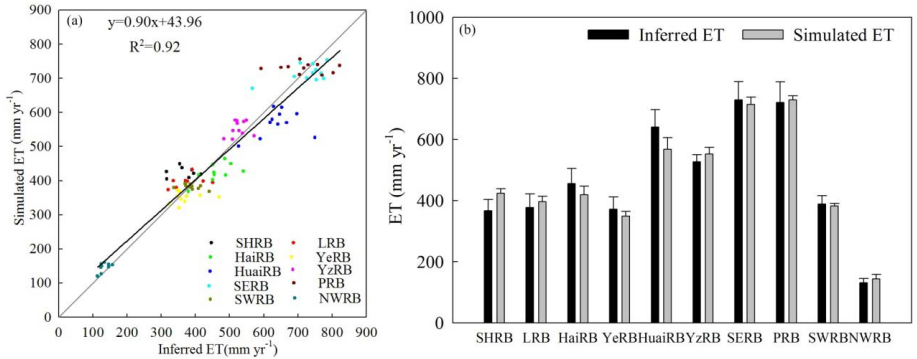

Fig. 5. Comparison of basin-level annual ET simulated by the BEPS model (Simulated ET) with that inferred using the water yield method (Inferred ET) in 10 basins during the period from 2000 to 2010. **(a)**: the comparison of data in all individual years and basins lumped together and the **(b)**: the comparison of simulated and inferred ET averaged over the study period in 10 basins.

HESSD
10, 5397–5456, 2013

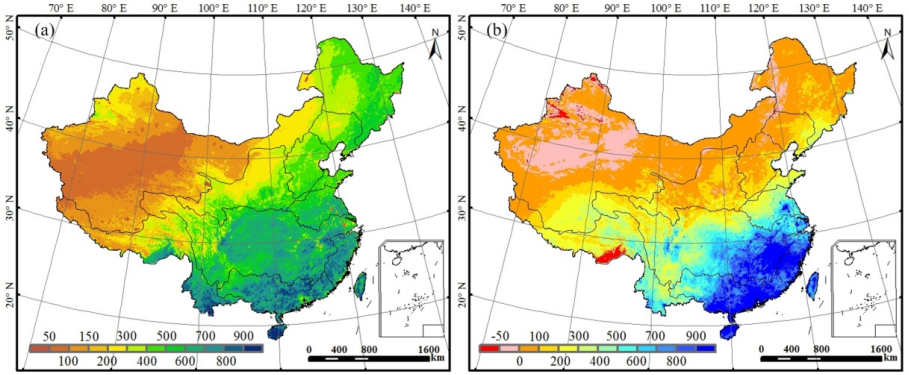

Fig. 6. The spatial distribution of mean annual ET **(a)** and water yield **(b)** during the period from 2000 to 2010.

HESSD
10, 5397–5456, 2013

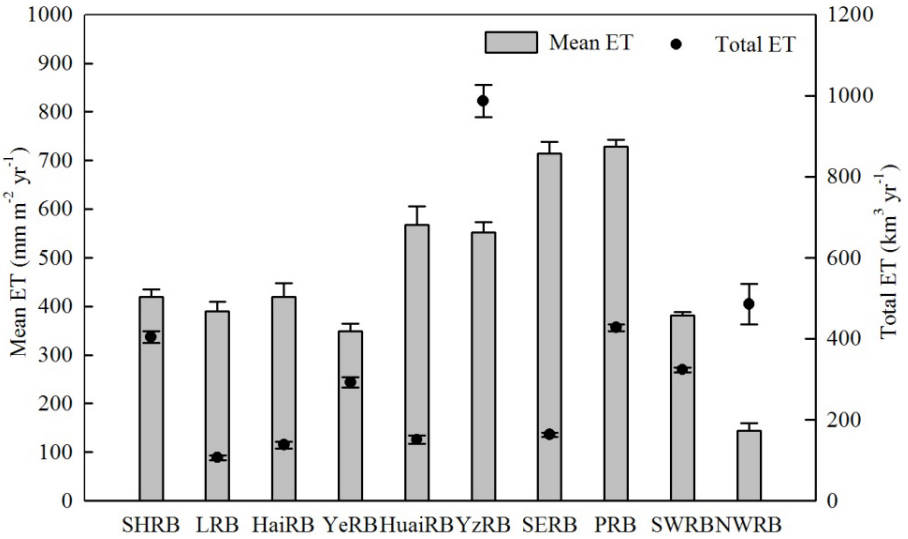

Fig. 7. The annual mean and total ET averaged over the period from 2000 to 2010 in 10 river basins.

HESSD
10, 5397–5456, 2013

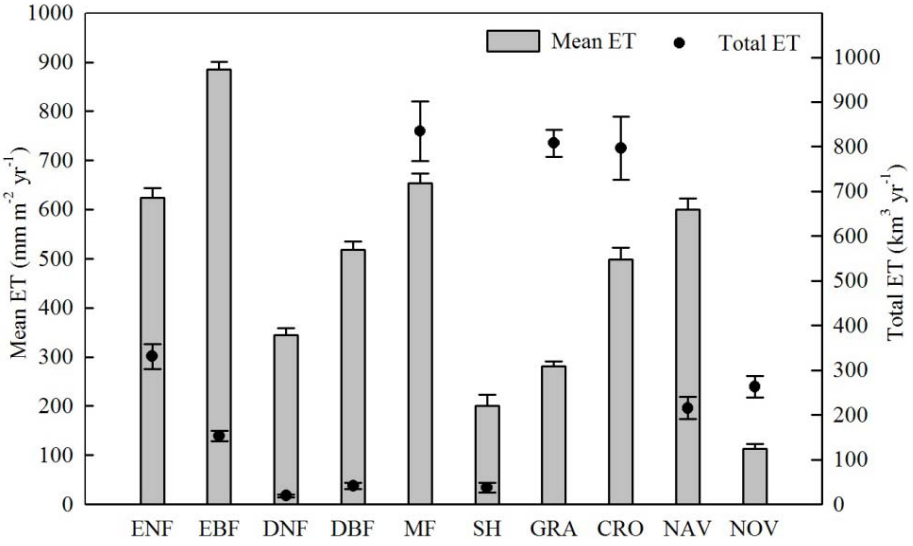

Fig. 8. Mean ET and total ET of different land cover types during the period from 2000 to 2010.

HESSD
10, 5397–5456, 2013

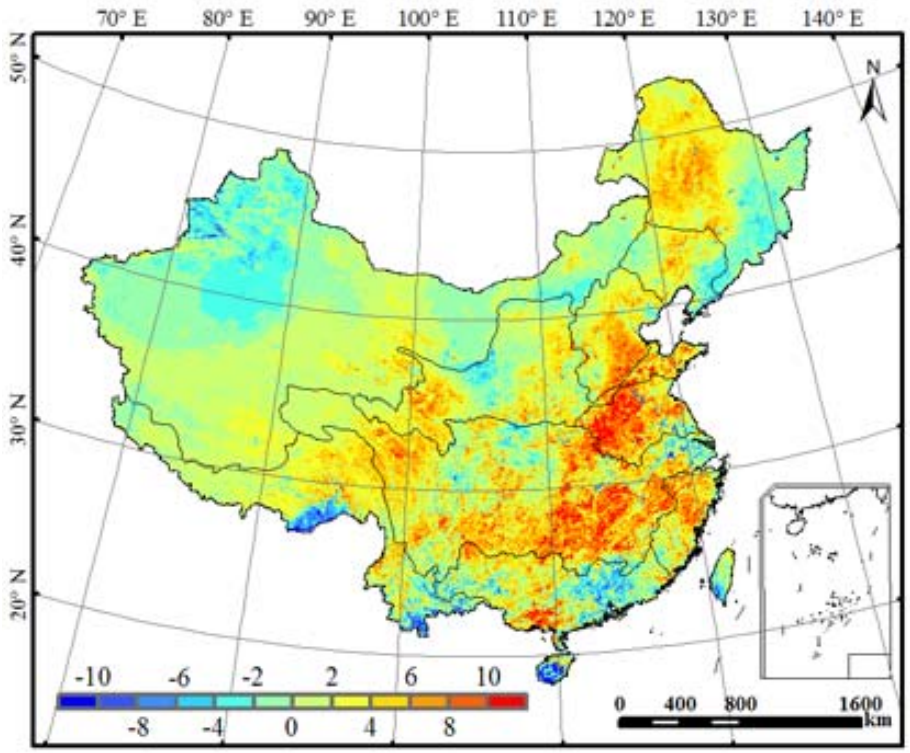

Fig. 9. Temporal trends of annual ET in China during the period from 2000 to 2010. Negative values indicate decreasing trends, vice versa.

HESSD
10, 5397–5456, 2013

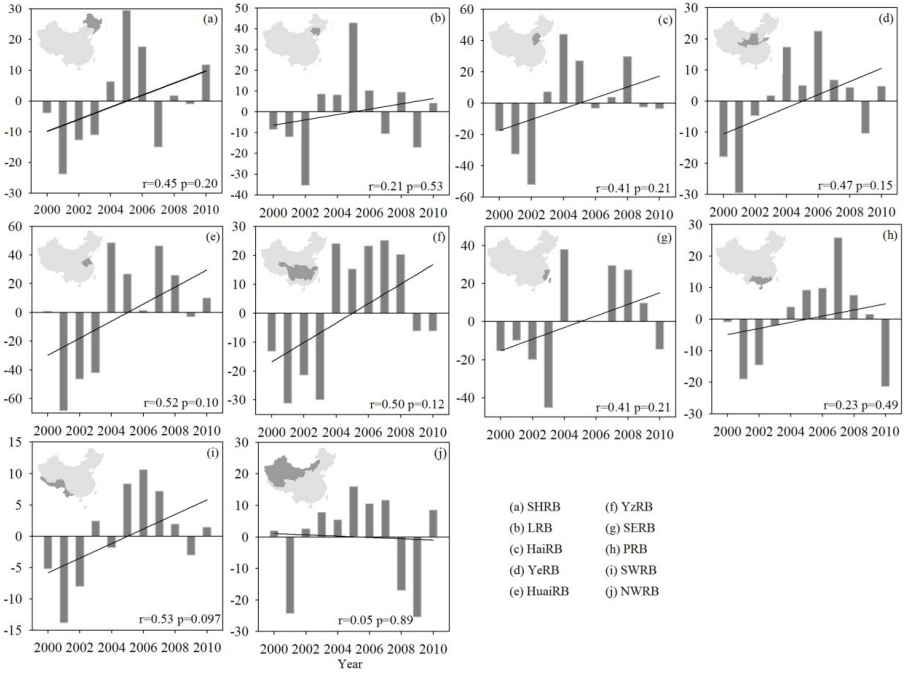

Fig. 10. The departures of annual ET from multiyear means in 10 basins during the period from 2000 to 2010.

HESSD
10, 5397–5456, 2013

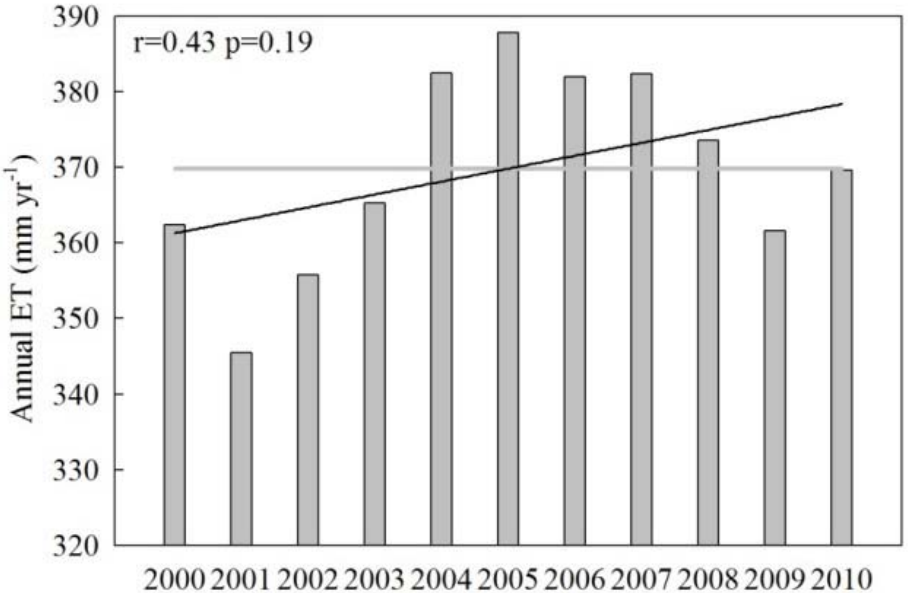

Fig. 11. National averages of annual ET in the terrestrial ecosystems of China during the period from 2000 to 2010.

HESSD
10, 5397–5456, 2013

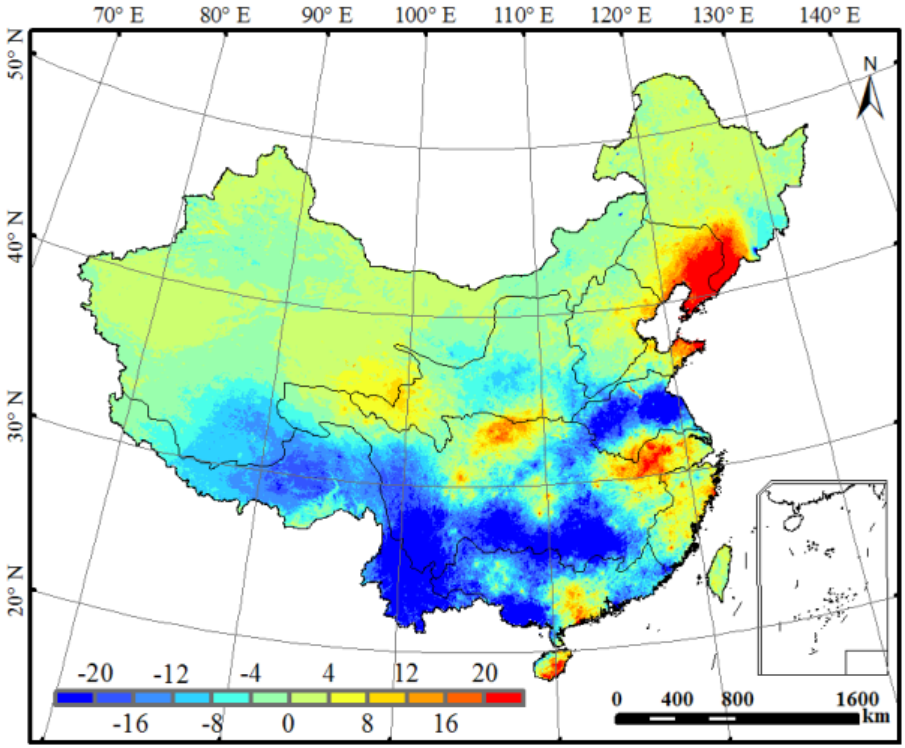

Fig. 12. Temporal trends of water yield in China from 2000 to 2010. Negative values indicate decreasing trends, vice versa.

HESSD
10, 5397–5456, 2013

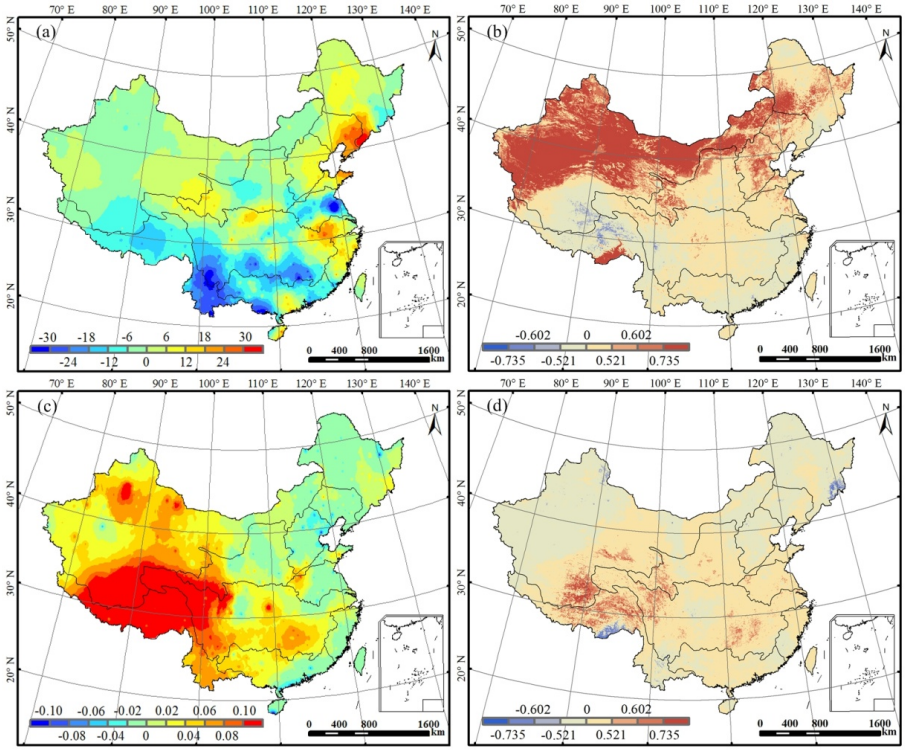

Fig. 13. Temporal trends of annual precipitation ($mm\,yr^{-1}$) **(a)** and mean annual temperature (MAT) ($^{\circ}C\,yr^{-1}$) **(c)** and the correlation coefficients of annual precipitation **(b)** and MAT **(d)** with annual ET during the period from 2000 to 2010. Negative values indicate decreases or negative correlations, vice versa. The values of 0.521, 0.602, and 0.735 for correlation coefficients represent the 0.10, 0.05, and 0.01 significance levels, respectively.

HESSD
10, 5397–5456, 2013

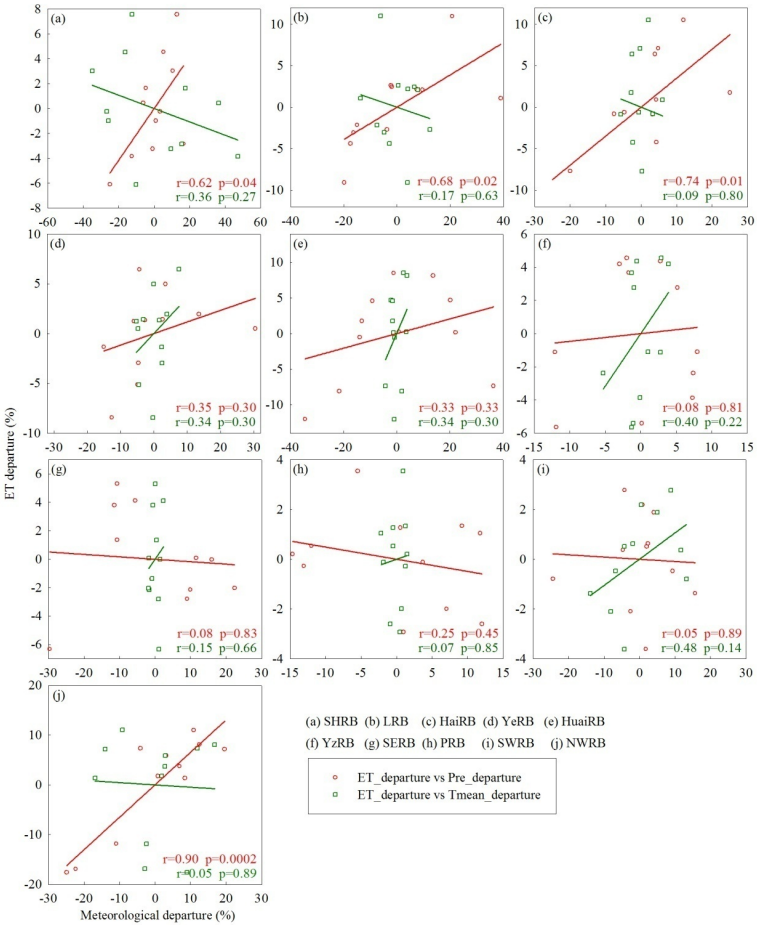

Fig. 14. The correlations between the departures of basin-level mean annual ET and climatic factors (precipitation, temperature).

HESSD
10, 5397–5456, 2013

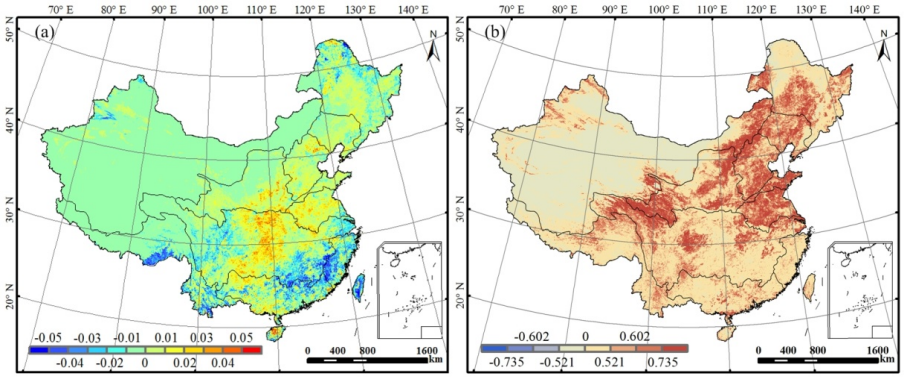

Fig. 15. Temporal trends of LAI **(a)** and the correlation coefficients of annual mean LAI with annual ET **(b)** during the period from 2000 to 2010. Negative values indicate decreases or negative correlations, vice versa. The values of 0.521, 0.602, and 0.735 for correlation coefficients represent the 0.10, 0.05, and 0.01 significance levels, respectively.

HESSD
10, 5397–5456, 2013